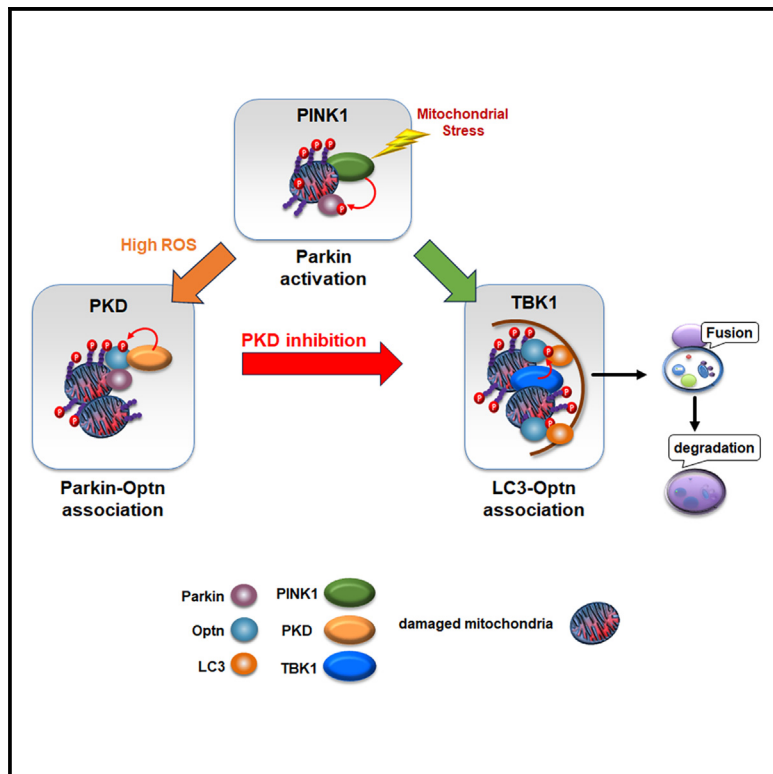


Phosphorylation of Optineurin by protein kinase D regulates Parkin-dependent mitophagy

Graphical abstract



Authors

Robert Weil, Emmanuel Laplantine, Messaouda Attailia, ..., Aya Yokota, Elie Banide, Pierre Génin

Correspondence

pierre.genin@sorbonne-universite.fr

In brief

Molecular biology; Cell biology

Highlights

- Protein kinase D are activated and recruited to mitochondria during mitophagy
- PKD kinases phosphorylate Optn that interacts with Parkin, enhancing its activity
- Inhibiting PKD boosts Optn-LC3 interaction and Parkin recruitment to mitochondria
- PKD inhibition leads to increased ROS production and reduced mitochondrial mass



Article

Phosphorylation of Optineurin by protein kinase D regulates Parkin-dependent mitophagy

Robert Weil,¹ Emmanuel Laplantine,^{1,5} Messaouda Attailia,^{2,5} Anne Oudin,¹ Shannel Curic,³ Aya Yokota,⁴ Elie Banide,³ and Pierre Génin^{1,6,*}

¹Centre d'Immunologie et des Maladies Infectieuses, CIMI-Paris, Sorbonne Université UMRS CR7 - Inserm U1135 - CNRS EMR8255, Faculté de Santé, 91 Boulevard de l'Hôpital, F-75013 Paris, France

²Université d'Orléans, UFR Sciences et Techniques, 45100 Orléans, France

³Université Paris-Saclay, Faculté de Médecine, 91190 Gif-sur-Yvette, France

⁴Sorbonne Université, Faculté des Sciences et Ingénierie, 75005 Paris, France

⁵These authors contributed equally

⁶Lead contact

*Correspondence: pierre.genin@sorbonne-universite.fr

<https://doi.org/10.1016/j.isci.2024.111384>

SUMMARY

Degradation of damaged mitochondria, a process called mitophagy, plays a role in mitochondrial quality control and its dysfunction has been linked to neurodegenerative pathologies. The PINK1 kinase and the ubiquitin ligase Parkin-mediated mitophagy represents the most common pathway in which specific receptors, including Optineurin (Optn), target ubiquitin-labeled mitochondria to autophagosomes. Here, we show that Protein Kinases D (PKD) are activated and recruited to damaged mitochondria. Subsequently, PKD phosphorylate Optn to promote a complex with Parkin leading to enhancement of its ubiquitin ligase activity. Paradoxically, inhibiting PKD activity enhances the interaction between Optn and LC3, promotes the recruitment of Parkin to mitochondria, and increases the mitophagic function of Optn. This enhancement of mitophagy is characterized by increased production of mitochondrial ROS and a reduction in mitochondrial mass. The PKD kinases may therefore regulate Optn-dependent mitophagy by amplifying the Parkin-mediated degradation signals to improve the cell response against oxidative stress damage.

INTRODUCTION

Mitophagy is the selective degradation of defective mitochondria by autophagy, mainly following damage and cellular stress, including oxidative stress that develops when the cellular redox balance is disturbed by an excessive build-up of reactive oxygen species (ROS). All types of mitophagy follow a general pattern involving receptors that physically connect the mitochondria to autophagosomes.¹ The nature and origin of mitophagy receptors can vary depending on the type of mitophagy: some receptors are proteins or lipids localized in the mitochondrial membrane, while others are non-mitochondrial proteins.² The best-known mitophagy pathway requires catalytic activities of the phosphatase/tensin homolog-induced kinase 1 (PINK1) and the cytosolic E3 ubiquitin ligase Parkin.^{3,4} Following mitochondrial damage, PINK1 is stabilized on the outer membrane of damaged mitochondria and recruits Parkin to the mitochondria. Thereafter, Parkin ubiquitinates outer membrane proteins,⁵ and in turn recruits specific receptors including p62/SQSTM1 (p62), neighbor of BRCA1 (NBR1), nuclear dot protein 52 (NDP52/CALCOCO2), Tax1 Binding Protein 1 (Tax1BP1) and Optineurin (Optn) that stably associate with ubiquitinated mitochondria via their Ubiquitin-binding domains (UBDs). These receptors subsequently associate with autophagosomal proteins such as GABARAP/LC3

family members, via a domain called LC3-interacting region (LIR), leading to formation of an autophagosome vesicle that engulfs damaged mitochondria. It was first reported that Optn is actively recruited to Parkin-positive mitochondria and stabilized by its ubiquitin-binding domain.⁶ Accordingly, another study showed that Optn, NDP52, as well as TAX1BP1 are recruited to mitochondria with similar kinetics following either mitochondrial depolarization or localized generation of ROS, leading to mitochondria sequestration by the autophagosome.⁷ Using pentaKO HeLa cells, in which five endogenous autophagy receptors (p62, NBR1, NDP52, Tax1BP1 and Optn) were depleted by CRISPR/Cas9 approaches, it was observed that all five individually re-expressed receptors are recruited to damaged mitochondria, but only re-expression of Optn and NDP52 (and Tax1BP1 to a lesser extent) could rescue mitophagy.^{5,8} In agreement with a critical role of Optn and NDP52, it was shown that the UBD of Optn and NDP52 controls their mitochondrial recruitment and that artificial targeting of PINK1 to the OMM of undamaged mitochondria in Parkin-depleted cells was sufficient to promote recruitment of both proteins and low levels of mitophagy.⁵

The TRAF family member-associated NF-κB activator (TANK)-binding kinase-1 (TBK1) has been shown to act as an upstream regulator of mitophagy. TBK1 is activated following mitophagy induction and is recruited together with Optn on depolarized



damaged mitochondria.⁷ Activated TBK1 then phosphorylates Optn at S177 to promote its interaction with LC3 and GABARAP family members localized at the autophagosomal membranes and to ensure subsequent autophagy of bacteria, protein aggregates or mitochondria.^{5,8–10} Proteomic analyses later demonstrated that TBK1 phosphorylates Optn on two additional sites, S473 and S513, enhancing ubiquitin binding and retention on damaged mitochondria.¹¹ Strikingly, S473 phosphorylation of Optn by TBK1 increases its affinity toward all ubiquitin chain types, especially when Ub is phosphorylated on S65 (S65-Ub).¹¹ TBK1 also phosphorylates NDP52, p62 and Tax1BP1 on multiple autophagy-relevant sites, including the UBD of p62, SKICH domains of NDP52 and Tax1BP1 and LIR domains of p62.^{4,11,12} However, expression of a triple mutated version of Optn on all S177, S473 and S513 residues in “penta KO” cells (depleted for five autophagy receptors) did not severely impaired mitophagy, arguing for other regulatory mechanisms in addition to phosphorylation by TBK1.¹¹

Protein kinases D (PKD) are a family of serine/threonine protein kinases (PKD1, PKD2, PKD3), encoded by three different genes: PKD1/PKC μ , PKD2 and PKD3/PKC ν , that belong to the Ca²⁺/calmodulin-dependent protein kinase (CAMK) group of Ser/Thr kinases.¹³ PKD kinases phosphorylate a variety of substrates such as CERT, Cortactin, CREB, DLC-1, HDAC5 and 7, Hsp27 TLR5 and Vps34, the latter being involved in the formation of the autophagosome, suggesting a regulatory role in autophagy. Indeed, under moderate oxidative stress, the death-associated protein kinase (DAPK) phosphorylates PKD1 which, in turn, activates the VPS34-Beclin1 complex involved in the interaction and maturation of the autophagosome.¹⁴

Under oxidative stress conditions that lead to mitophagy, PKD activation is initiated by mitochondrial diacylglycerol production through phospholipase D and phosphatidic acid phosphatase activities.¹⁵ Once activated, PKD kinases regulate several pathways downstream of oxidative stress including the nuclear factor kappa-light-chain-enhancer of the activated B cell (NF- κ B). This activation results in upregulation of manganese superoxide dismutase (mnSOD) that detoxifies cells from mitochondrial-generated ROS, but also generates H₂O₂, a tumor-promoting signaling molecule.¹⁶ In neuronal cells, the PKD/NF- κ B/SOD2 axis is constitutively active and protects against oxidative damage. Oxidative stress-induced PKD1 can also activate Jun N-terminal Kinase, downstream of death-associated protein kinase (DAPK), leading not only to increased autophagy, but also to pro-death signaling.¹⁴

In cardiac myoblasts and rat neonatal cardiomyocytes, G_q protein-coupled receptor (G_qPCR) stimulation induces PKD translocation from the cytoplasm to the outer mitochondrial membrane to phosphorylate the mitochondrial fission protein, dynamin-like protein 1 (DLP1).¹⁷ This event further initiates DLP1 association with the OMM, which enhances mitochondrial fragmentation, superoxide generation, permeability transition pore opening and apoptotic signaling. Optineurin and PKD kinases being both involved in autophagy, mitochondrial dynamics, Golgi apparatus maintenance and membrane trafficking, we decided to explore their relationship.¹⁸

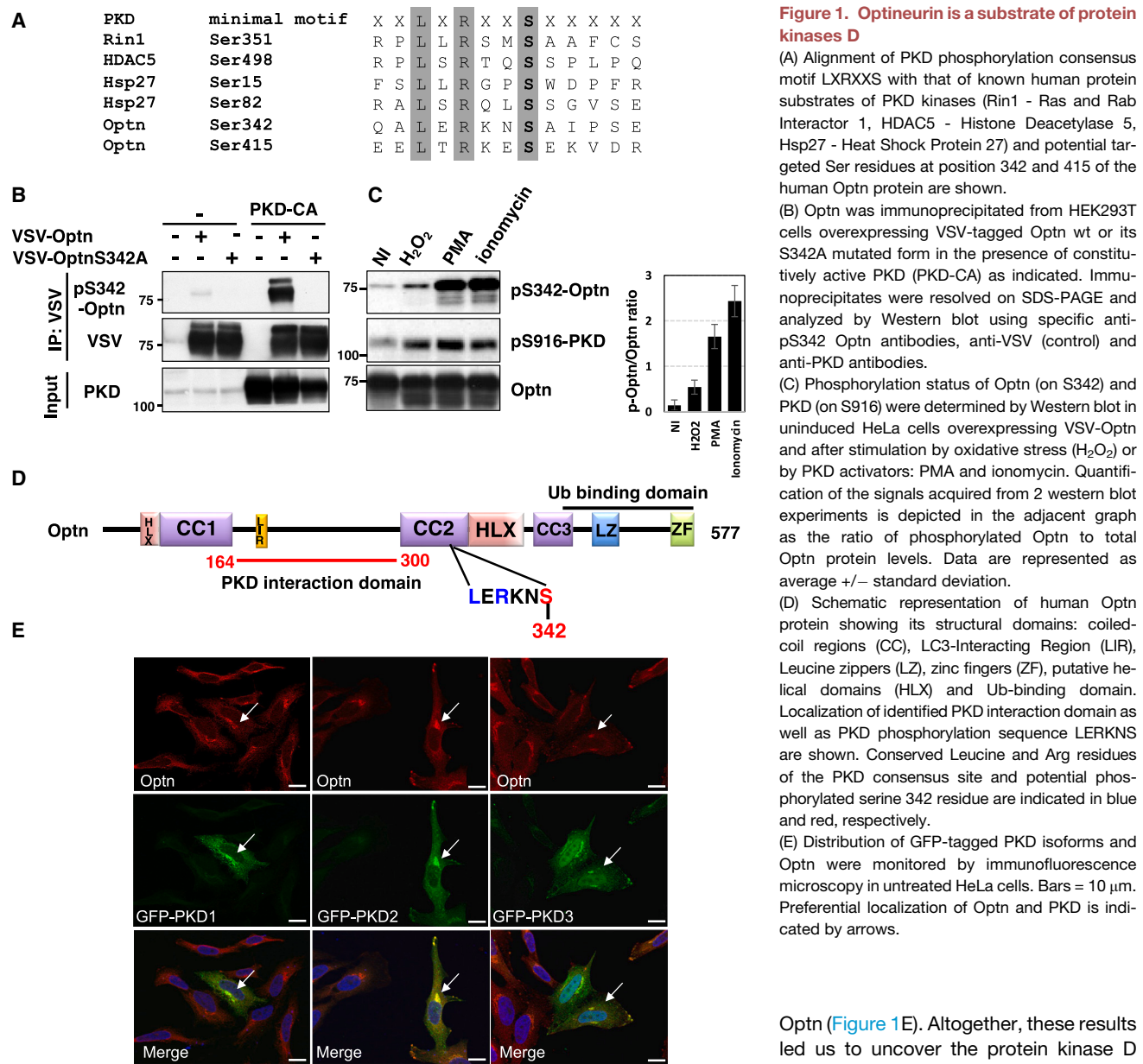
In the present study, we identify Optn as a substrate and protein interactant of the Protein Kinase D (PKD) family members.

We showed that Optn is phosphorylated on Ser 342 in response to PKD activating stimuli, but also at early steps of mitophagy. Interestingly, we observed that PKD is activated and recruited to damaged mitochondria during mitophagy in a Parkin dependent manner. We also demonstrated that Optn phosphorylation by PKD during mitophagy induces its complex formation with Parkin. Importantly, we found that Parkin activity is enhanced by PKD pathway activation as monitored by Parkin S65 and ubiquitin S65 phosphorylations. PKD activation was also found to impede the recruitment of Parkin to mitochondria and counteract Optn’s interaction with LC3, thereby delaying the completion of mitophagy. Overall, our data show that PKD kinases are involved in the amplification of the recognition signal of damaged mitochondria by ubiquitin, ultimately leading to an extension of the mitophagic process.

RESULTS

Optineurin is a substrate of protein kinase D

In search of kinases that could regulate Optn functions, we identified two phosphorylation sites for PKD kinase family (serine/threonine-protein kinase D) matching the minimal consensus motif LXRXS on human Optn protein sequence, with putative targeted Ser residues at position 342 and 415, respectively (Figure 1A). Sequence alignment of Optn from different species showed that S342 residue is conserved among Human, Macaque, Rat and Mouse, while S415 residue is present only in Human and Macaque. To determine whether PKD could phosphorylate Optn on these sites, we performed *in vitro* kinase assays using as substrates GST-Optn wt or mutated constructs GST-Optn-S342A and S415A, in which the putative serine residues were replaced by Alanine and immunoprecipitated PKD as a source of kinase (Figures S1A and S1B). We observed that PKD could phosphorylate Optn wt and Optn S415A, but not constructs that carry the S342A mutation (Figure S1C). No additional increase in Optn phosphorylation was observed with Phorbol Myristate Acetate (PMA) and ionomycin treatment suggesting either that activating agents could have been washed away during the immunoprecipitation steps or that overexpressed PKD1 was already in an active state and could not be significantly further activated. Interestingly, phosphorylated Optn was also detected in cells stimulated by PMA/Ionomycin following immunoprecipitation of endogenous PKD (Figure S1D). As expected, pre-treatment with staurosporine, an S/T kinase inhibitor, resulted in the disappearance of phosphorylated Optn. In addition, phosphorylated Optn could be detected using anti-Phospho-(Ser/Thr) PKD substrate antibodies (pMotif) following immunoprecipitation of Optn, in cells expressing Optn wt, but not Optn-S342A (Figure S1E). As expected, the pMotif antibody could recognize the phosphorylation of Optn in cells co-expressing constitutively active form (CA), but not a kinase-dead form (DN) of PKD. To further investigate the phosphorylation of Optn at Ser342, we generated a rabbit polyclonal phospho-specific antibody raised against the peptide epitope surrounding the S342 residue of Optn. This antibody detected Optn wt, but not the S342A mutant, when co-expressed with PKD CA (Figure 1B). Using this antibody, we also found that overexpressed Optn was phosphorylated following activation of PKD by oxidative stress



(H_2O_2) or by well-known PKD activators such as PMA/ionomycin (Figure 1C). Coimmunoprecipitation assays were used to study the interaction between PKD and its substrate Optn. We found that PKD CA interacts with Optn wt and S342A, while the kinase dead mutant of PKD (DN) only weakly interacted compared to active PKD (Figures S2A and S2C). Similar experiments performed using N- and C-terminal deleted constructs demonstrated that the [aa 164–300] region of Optn includes the interaction domain between Optn and PKD (Figures S2B and S2C and Figure 1D). We performed immunofluorescence staining in HeLa cells expressing GFP-tagged version of the three members of PKD family (PKD1/PKC μ , PKD2 and PKD3/PKC ν) and observed that they displayed the same cellular localization as endogenous

Figure 1. Optineurin is a substrate of protein kinases D

(A) Alignment of PKD phosphorylation consensus motif LXRXS with that of known human protein substrates of PKD kinases (Rin1 - Ras and Rab Interactor 1, HDAC5 - Histone Deacetylase 5, Hsp27 - Heat Shock Protein 27) and potential targeted Ser residues at position 342 and 415 of the human Optn protein are shown.

(B) Optn was immunoprecipitated from HEK293T cells overexpressing VSV-tagged Optn wt or its S342A mutated form in the presence of constitutively active PKD (PKD-CA) as indicated. Immunoprecipitates were resolved on SDS-PAGE and analyzed by Western blot using specific anti-pS342 Optn antibodies, anti-VSV (control) and anti-PKD antibodies.

(C) Phosphorylation status of Optn (on S342) and PKD (on S916) were determined by Western blot in uninduced HeLa cells overexpressing VSV-Optn and after stimulation by oxidative stress (H_2O_2) or by PKD activators: PMA and ionomycin. Quantification of the signals acquired from 2 western blot experiments is depicted in the adjacent graph as the ratio of phosphorylated Optn to total Optn protein levels. Data are represented as average +/- standard deviation.

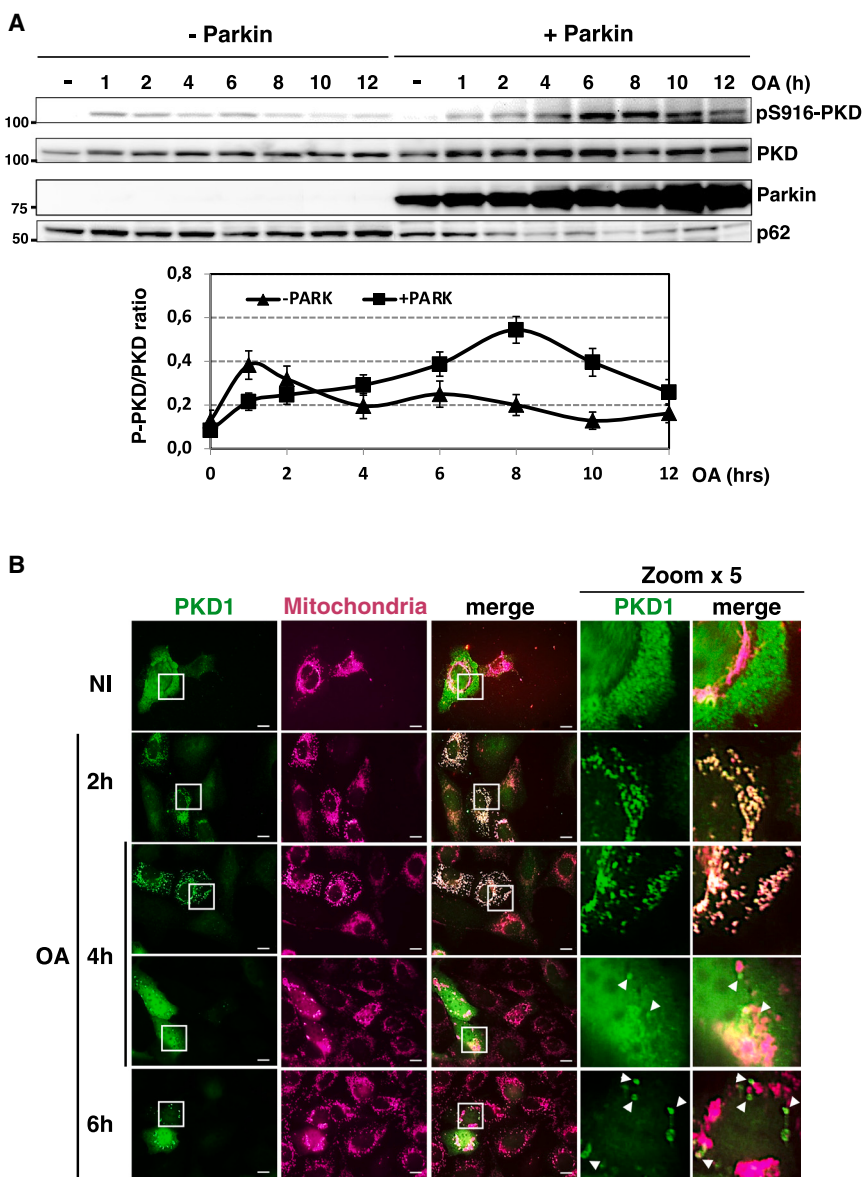
(D) Schematic representation of human Optn protein showing its structural domains: coiled-coil regions (CC), LC3-Interacting Region (LIR), Leucine zippers (LZ), zinc fingers (ZF), putative helical domains (HLX) and Ub-binding domain. Localization of identified PKD interaction domain as well as PKD phosphorylation sequence LERKNS are shown. Conserved Leucine and Arg residues of the PKD consensus site and potential phosphorylated serine 342 residue are indicated in blue and red, respectively.

(E) Distribution of GFP-tagged PKD isoforms and Optn were monitored by immunofluorescence microscopy in untreated HeLa cells. Bars = 10 μm . Preferential localization of Optn and PKD is indicated by arrows.

Optn (Figure 1E). Altogether, these results led us to uncover the protein kinase D family members as novel protein interactants and kinases of Optn. Since PKD kinases, actors of the oxidative stress pathways, have been involved in the autophagic process and linked to mitochondria fragmentation and dysfunction, we hypothesized that these kinases could regulate the function of Optn during the mitophagy process.^{14,17}

Protein kinases D are activated and recruited to damaged mitochondria during mitophagy

We first assessed whether PKD kinases are activated and recruited to mitochondria during mitophagy. To determine the effect of mitophagy on PKD activity, we used combination of oligomycin and antimycin A (OA) to depolarize mitochondria, as this treatment was reported to initiate mitophagy by inhibiting mitochondrial respiration and impairing mitochondrial



homeostasis.¹⁹ We examined PKD autophosphorylation (S916) by Western blot, during OA treatment in parental or Parkin-expressing HeLa cells. PKD phosphorylation was only slightly and transiently induced in parental HeLa cells, while exogenous expression of Parkin resulted in high and sustained PKD activity (Figure 2A and quantification below). As expected, expression levels of the autophagic receptor p62 (a control of mitophagy efficiency²⁰), were barely affected in parental HeLa cells, but strongly degraded in Parkin-expressing cells along the course of mitophagy induction. Interestingly, we also found that depletion of Optn expression resulted in the inhibition of the OA-induced PKD activation (Figure S3A).

PKD kinases exert their biological functions depending on their cellular localization: at the plasma membrane, in the cytoplasm and in association with the Golgi apparatus or in the nucleus.¹⁸ We thus perform immunofluorescence staining to determine the

Figure 2. Protein kinases D are activated and recruited to damaged mitochondria during mitophagy

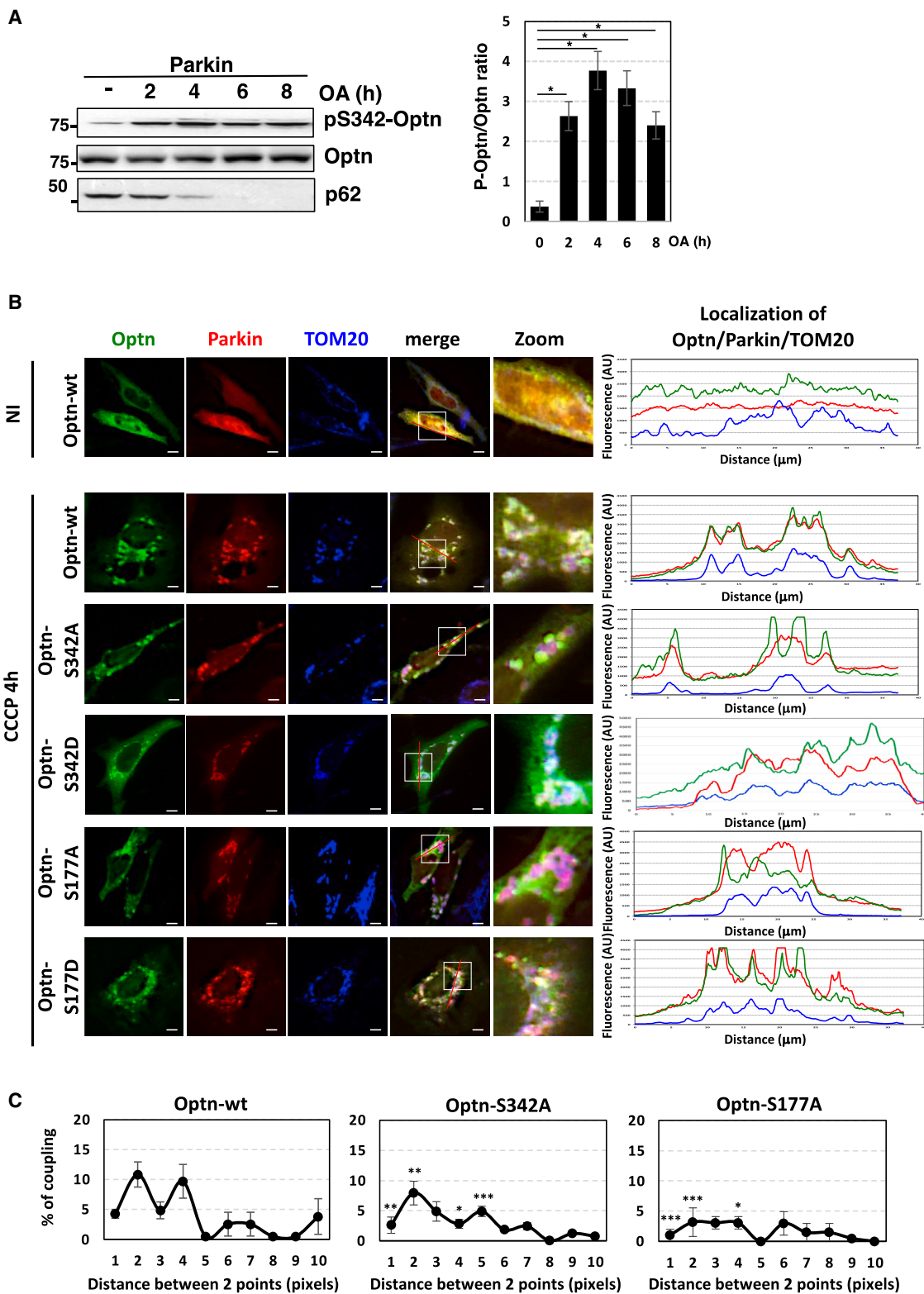
(A) Total cell lysates from HeLa cells expressing empty vector or BFP-tagged Parkin harvested at different time after mitophagy induced by the combination of oligomycin and antimycin A (OA), were analyzed by Western blot using anti-pS916 PKD, PKD, Parkin and p62 antibodies. The quantification of the ratio of phosphorylated PKD to total PKD protein levels obtained from 3 independent western blot experiments is illustrated in the graph below. Data are represented as average +/- standard deviation.

(B) Changes in localization of GFP-tagged PKD1 were monitored by immunofluorescence microscopy in non-induced (NI) HeLa cells stably expressing Parkin or following OA treatment for 2, 4 or 6h. Mitochondria were labeled using MitoTracker. Bars = 10 μ m. Arrows indicate round shaped structures resembling autophagosomes, surrounding or located close to mitochondria aggregates.

localization of PKD during mitophagy. We observed that overexpressed PKD1 displayed cytosolic distribution before induction, but was observed as punctuated dots at both 2 and 4h of OA treatment, and was also present as round shaped structures resembling autophagosomes and located close to mitochondria aggregates, after 4 and 6h of induction (Figure 2B). To further characterize these structures, we analyzed LC3 localization by immunofluorescent microscopy in HeLa cells stably expressing BFP-Parkin and transiently transfected with GFP-PKD. The results demonstrated clear colocalization between PKD/Parkin punctuated signals and LC3 dots (Figure S3C, left panel, white arrows). Similar experiments with GFP-PKD2 and GFP-PKD3 further confirmed that not only PKD1, but also PKD2 and PKD3 are recruited to Parkin aggregates during mitophagy. Several of the observed PKD/Parkin signals colocalized with LC3 staining (Figure S3C, right and lower panels, white arrows). Altogether these data clearly indicate that PKD1 is activated and recruited to mitochondria during mitophagy.

PKD control the coupling between Parkin and Optn

We next address the role of the Ser342 phosphorylation of Optn in mitophagy. First, we demonstrated that the S342 phosphorylation was increased during the course of mitophagy, starting as early as 2h of OA treatment as observed by western blot using phospho-specific pS342 antibodies (Figure 3A). Interestingly, unlike the PI3Kinase inhibitor 3-MA that abrogates OA-induced phosphorylation of Optn (comparison of lanes 3 and 1 of Figure S3B), treatment with the autophagosome-lysosome fusion inhibitor baflomycin did not affect Optn phosphorylation

**Figure 3. The S342 phosphorylation regulates Optn localization relative to Parkin**

(A) Total cell lysates from HeLa cells expressing BFP-tagged Parkin and transfected with VSV-Optn were harvested at different time after mitophagy induction by OA and analyzed by Western blot using anti-pS342 Optn, Optn and p62 antibodies. Quantification of the signals acquired from 3 independent western blot

(legend continued on next page)

(comparison of lanes 3 and 2 of **Figure S3B**). Moreover, this phosphorylation was not changed by the expression of a catalytic inactive form of Parkin (Parkin-C431S) that blocks mitophagy as monitored by impaired p62 degradation (comparison of lanes 5 and 3 of **Figure S3B**). These results indicate that the Optn S342 phosphorylation occurs at early stages of the mitophagy process and does not require Parkin activity.

Second, we assessed the effect of Optn phosphorylation on its recruitment to damaged mitochondria, by determining the localization of overexpressed wild-type and Optn-S342A by fluorescent microscopy (**Figures 3B** and **S4** for replicates). As expected, Optn wt and Parkin were uniformly distributed in the cytoplasm of untreated cells, but both proteins were recruited to mitochondria (labeled with TOM20 antibodies) following mitophagy induction by CCCP (protonophore carbonyl cyanide *m*-chlorophenyl hydrazone). Line scan analysis of images (graph on the right) confirmed the complete overlap of the three signals of Parkin (red), Optn wt (green) and TOM20 (blue) following mitophagy induction (**Figure 3B**, second row). The Optn-S342A mutant exhibited a distinct mitochondrial distribution compared to Parkin and TOM20 in response to CCCP induction, but appears to be still recruited to damaged mitochondria. This difference is evidenced by the line scan graph, where the green line deviates from the red and blue lines. Notably, positioning of Parkin relative to TOM20 was unaffected by Optn S342A mutation. Interestingly, phosphomimetic mutation by an aspartic acid residue of S342 (S342D), partially restored the alignment of signals between Optn, Parkin, and TOM20 (**Figure 3B**, third row). Localization of Optn-S177A (that prevents phosphorylation by TBK1) differed also from that of Parkin and TOM20 (**Figure 3B**, fourth row), and its phosphomimetic mutation (S177D), partially restored the alignment of signals between Optn, Parkin, and TOM20 (**Figure 3B**, last row). To further understand the impact of these mutations on Optn recruitment to damaged mitochondria, we analyzed the images depicted in **Figures 3B** and **S4** using SODA (statistical object distance analysis) module (Icy software, Pasteur Institute) and focused on the average coupling between Optn and Parkin, both of which exhibit punctuated signals upon mitophagy induction (**Figure 3C**).²¹ In comparison to the coupling observed between Optn wt and Parkin, which typically ranged from 1 to 4 pixels, the coupling between the phosphodeficient mutants Optn-S342A/S177A and Parkin was significantly reduced (middle and right panels of **Figure 3C**). This finding lines up with previous observations showing reduced recruitment of

the S177A phosphodeficient mutant of Optn to mitochondria.⁵ To ascertain statistically significant differences in colocalization between Parkin and Optn wt or phosphodeficient mutants of Optn, we conducted confocal imaging experiments and analyzed the colocalization of Optn with Parkin (**Figure S5A** and graph). The results clearly illustrate a decreased overlap percentage between Optn and Parkin when mutated at the S342 or S177 residues, highlighting significant differences in their colocalization. Taken together, these results suggest that Optn phosphorylation modulates the co-recruitment of Optn and Parkin in close proximity on the surface of damaged mitochondria.

Parkin and Optn forms a complex regulated by PKD kinases

To further detail the impact of PKD-mediated phosphorylation on the Optn-Parkin association, we performed co-immunoprecipitation assays in HeLa cells overexpressing Parkin and VSV-tagged form of Optn wt (**Figure 4A**). Data obtained indicate a constitutive association between Optn and Parkin. Co-expression of PKD1 with Parkin and Optn resulted in a robust enhancement in the detection of Parkin within Optn immunoprecipitates, both in unstimulated and OA-treated cells. This observation suggests that PKD promotes the formation of the Parkin-Optn complex. To investigate the impact of the S342A mutation on Optn-Parkin complex formation, triple knockout (TKO) HeLa cells,⁵ in which Optn, NDP52, and Tax1BP1 were eliminated through CRISPR/CAS9 and TALEN approaches, were reconstituted with Optn variants. In these cells, the association between overexpressed Optn wt and Parkin, assessed following VSV-Optn immunoprecipitation, was only detected after mitophagy induction (**Figure 4B**, quantification in 4D, left panel). This association was reduced by the S342A mutation of Optn. Similarly, an inhibition of the Optn-Parkin complex was observed in the presence of a protein kinase D inhibitor (CID2011756),²² with the appearance of an upper band that correspond to either the autoubiquitylated or autoprophosphorylated forms of Parkin (**Figures 4B** and **4D**, left panel). Co-immunoprecipitation experiments performed in HeLa-TKO cells using either protein G-sepharose without immunoprecipitating antibodies or control IgG confirmed the specificity of the Parkin signal observed with anti-Optn immunoprecipitating antibodies (**Figure S3D**). These data suggest that phosphorylation of Optn by PKD during mitophagy promotes its association with native Parkin, but not its modified forms. Effects of the S342A mutation and PKD inhibition on Optn-Parkin

experiments is depicted in the adjacent graph as the ratio of phosphorylated Optn to total Optn protein levels. Data are represented as average \pm standard deviation. * $p < 0.05$ (OA vs. NI: 2h: $n = 3$, $\Delta = -3.40$, $t = -11.9$, $ddl = 2.33$, $p = 0.013$; 4h: $n = 3$, $\Delta = -2.26$, $t = -10.09$, $ddl = 2.56$, $p = 0.014$; 6h: $n = 3$, $\Delta = -2.963$, $t = -11.29$, $ddl = 2.40$, $p = 0.013$; 8h: $n = 3$, $\Delta = -2.032$, $t = -9.593$, $ddl = 2.63$, $p = 0.015$).

(B) Localization of Optn wt, phosphodeficient (S342A and S177A) or phosphomimetic mutants (S342D and S177D) of Optn and Parkin relative to mitochondria, were monitored by immunofluorescence microscopy in HeLa cells that were either left uninduced (NI) or stimulated by CCCP (Carbonyl cyanide *m*-chlorophenylhydrazone, respiratory chain uncoupler). Bars = 10 μ m. Images were analyzed by quantification of fluorescence intensity (arbitrary unit) of each channel over the distance indicated using line scans (Fiji software).

(C) The average statistical distance between Optn and Parkin was determined on images such as those presented in B, using the SODA ("Statistical Object Distance Analysis") statistical tool of the Icy software (Quantitative Image Analysis Unit, Institut Pasteur). The coupling percentage was calculated when both proteins are recruited to the surface of the mitochondria during mitophagy and is represented as a function of the distance (in pixels) between two fluorescent points. Data are represented as average \pm standard deviation. * $p < 0.05$, ** $p < 0.01$, *** $p < 0.001$ (S342A vs. WT, 1 pixel: $n = 6$, $\Delta = 1.67$, $t = 5.80$, $ddl = 9.61$, $p = 0.006$; 2 pixels: $n = 6$, $\Delta = 3.557$, $t = 6.323$, $ddl = 6.80$, $p = 0.009$; 4 pixels: $n = 6$, $\Delta = 7.03$, $t = 5.22$, $ddl = 5.28$, $p = 0.044$; 5 pixels: $n = 6$, $\Delta = -6.3967$, $t = -28.665$, $ddl = 5.00$, $p < 0.001$; S177A vs. WT, 1 pixel: $n = 6$, $\Delta = 4.27$, $t = 14.84$, $ddl = 9.61$, $p < 0.001$; 2 pixels: $n = 6$, $\Delta = 8.183$, $t = 14.546$, $ddl = 6.80$, $p < 0.001$; 4 pixels: $n = 6$, $\Delta = 8.471$, $t = 6.29$, $ddl = 5.28$, $p = 0.019$).

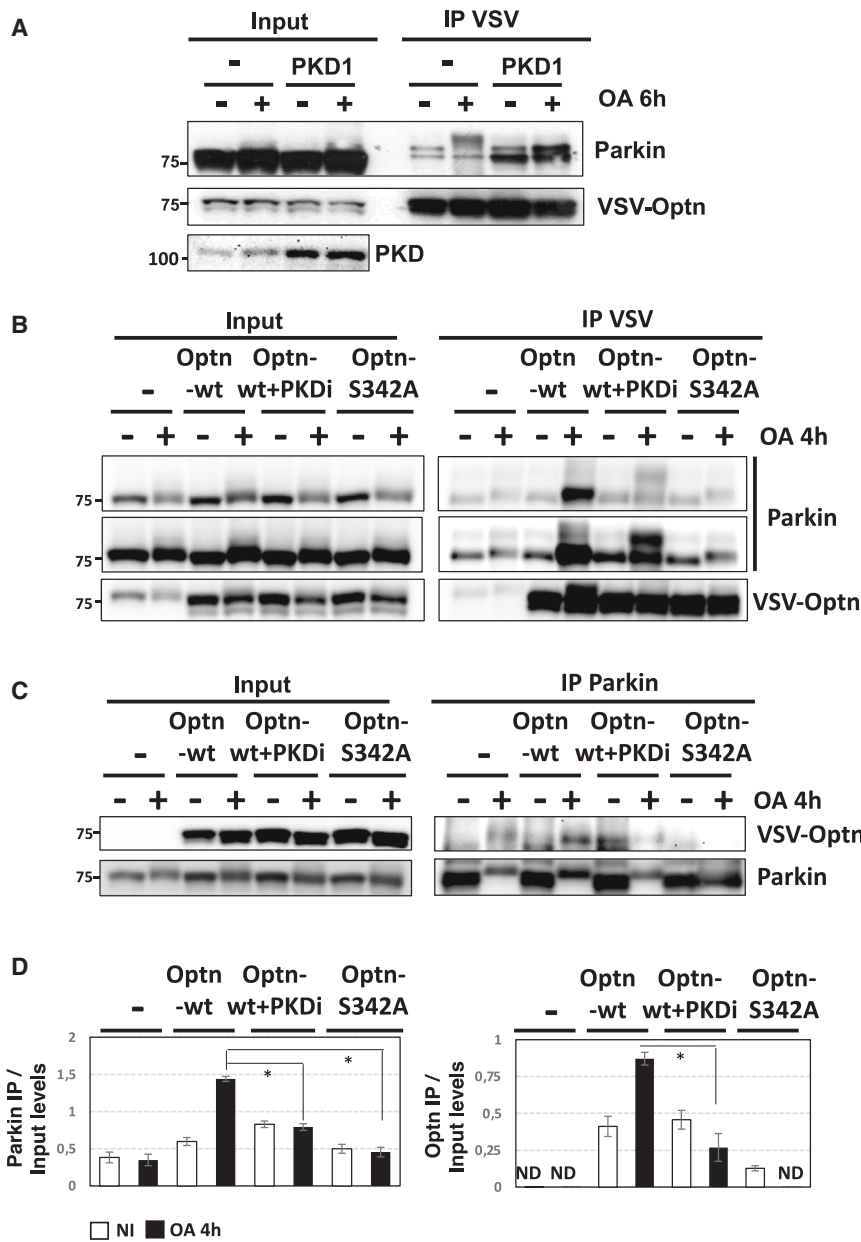


Figure 4. Parkin and Optn form a complex regulated by PKD kinases

(A) Optn was immunoprecipitated from HeLa cells overexpressing Parkin and transiently transfected with PKD1, as indicated. After transfection, cells were left untreated or treated with OA for 6h before lysis. Immunoprecipitates and Input (10% of the lysate used to perform the IP) were resolved on SDS-PAGE and analyzed by western blot using anti-Parkin, anti-VSV (control) and anti-PKD antibodies. The molecular masses (kDa) are represented on the left of each immunoblot.

(B and C) HeLa cells expressing Parkin were transiently transfected with VSV-tagged Optn wt or Optn-S342A, as indicated. After transfection, cells were treated with PKDi and OA, as indicated, lysed, and subjected to VSV (B) or Parkin (C) immunoprecipitation. Immunoprecipitates and Input (total lysate) were resolved on SDS-PAGE and analyzed by western blot using anti-Parkin and anti-VSV (control) antibodies. The molecular masses (kDa) are represented on the left of each immunoblot.

(D) Quantifications of the immunoprecipitation signals obtained from 2 independent experiments, as shown in B (left panel) and C (right panel), respectively, are illustrated as the ratio of Parkin/Optn following immunoprecipitation to total protein levels detected in total cell extracts (Input). Data are represented as average +/- standard deviation. ND, not determined. * $p < 0.05$, ** $p < 0.01$, *** $p < 0.001$ (in D: PKDi vs. wt $n = 2$, $\Delta = 0.708$, $t = 10.3$, ddl = 3.00, $p = 0.004$; S342A vs. wt $n = 2$, $\Delta = 1.041$, $t = 15.11$, ddl = 3.00, $p = 0.001$; in E: PKDi vs. wt $n = 2$, $\Delta = 0.515$, $t = 4.82$, ddl = 2, $p = 0.001$).

cells with OA further increased the number of Optn-Parkin dots per cell, as demonstrated by statistical analyses of the images (Figure S5B, lower panels, OA and graph below). These experiments revealed that these complexes are distributed throughout the cells rather than being confined to aggregated mitochondria. Their widespread distribution is likely due to the dispersion of Parkin in the cytoplasm, despite the selective

complex formation was confirmed in reverse co-immunoprecipitation assays, despite lower detection levels and a heightened background (Figures 4C and 4D, right panel).

The cellular distribution of the Optn-Parkin complexes was visualized by *in situ* Proximity Ligation Assays (PLA), which enable the detection of protein interactions by producing a distinct, localized signal. In control experiments (i.e., without one or the other primary antibody), only a few non-specific punctate signals were observed in HeLa cells stably expressing Parkin (Figure S5B, upper panels and graph below). In uninduced cells (Figure S5B, lower panels, NI), PLA performed with both antibodies revealed several dots, reminiscent of the constitutive Optn-Parkin complex formation observed in unstimulated Parkin-expressing HeLa cells (see Figure 4A). Treatment of

detection of Parkin to damaged mitochondria. Consistent with data from immunoprecipitation assays, treatment with PKDi, but not with TBK1 inhibitor (BX795), led to a significant reduction in the number of Optn-Parkin PLA dots. In summary, our findings suggest, for the first time, that Optn and Parkin interact in basal conditions and that this interaction is enhanced during mitophagy and facilitated by the phosphorylation of Optn by PKD.

We next assessed the effect of PKD activity on the interaction between Optn and LC3, that facilitates the autophagic degradation of damaged cellular components by linking them to the autophagosome machinery (Figure 5A). In *in situ* proximity ligation assays, the Optn-LC3 complexes are detected under uninduced conditions, likely reflecting the constitutive affinity of Optn for

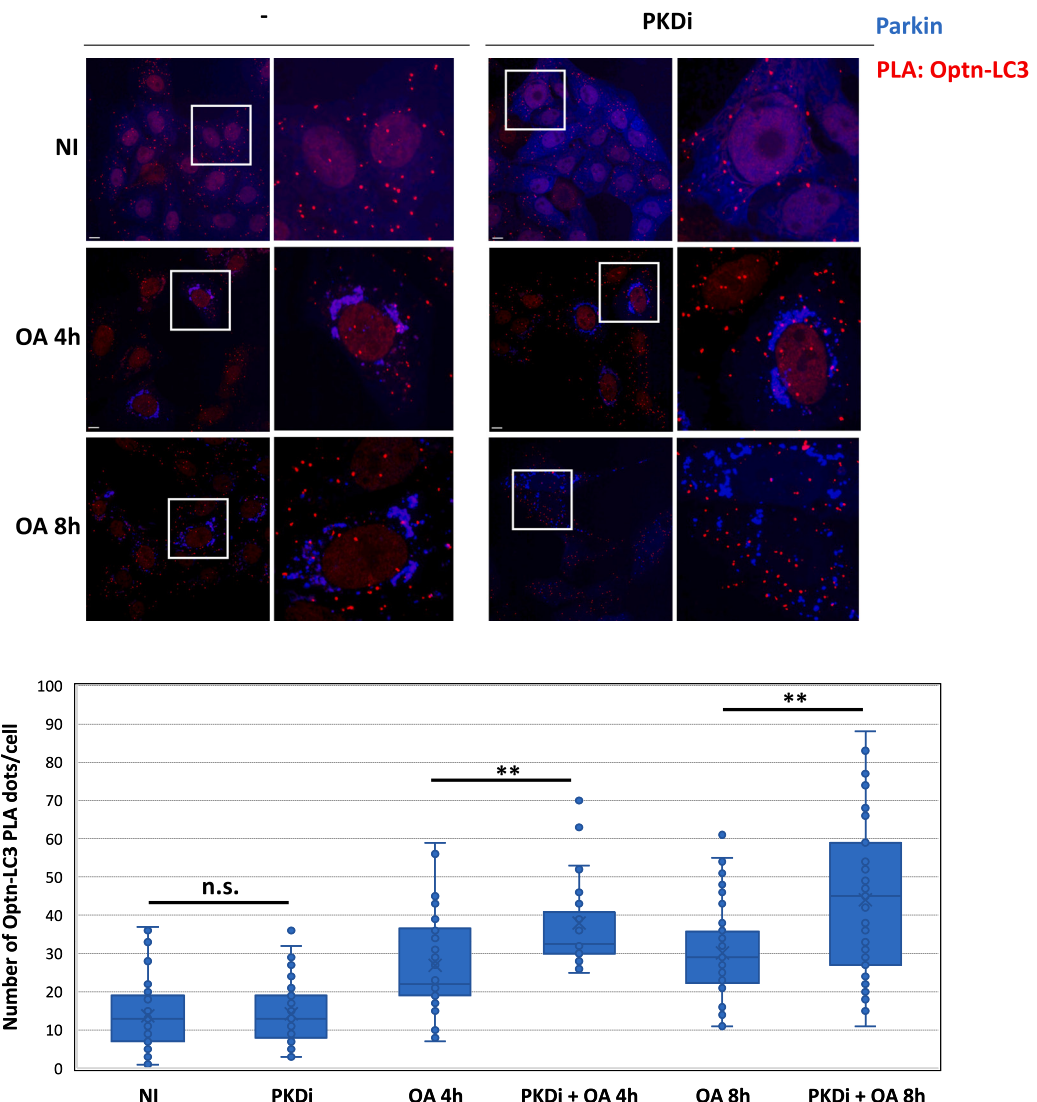


Figure 5. PKD inhibition enhances Optn-LC3 complex formation

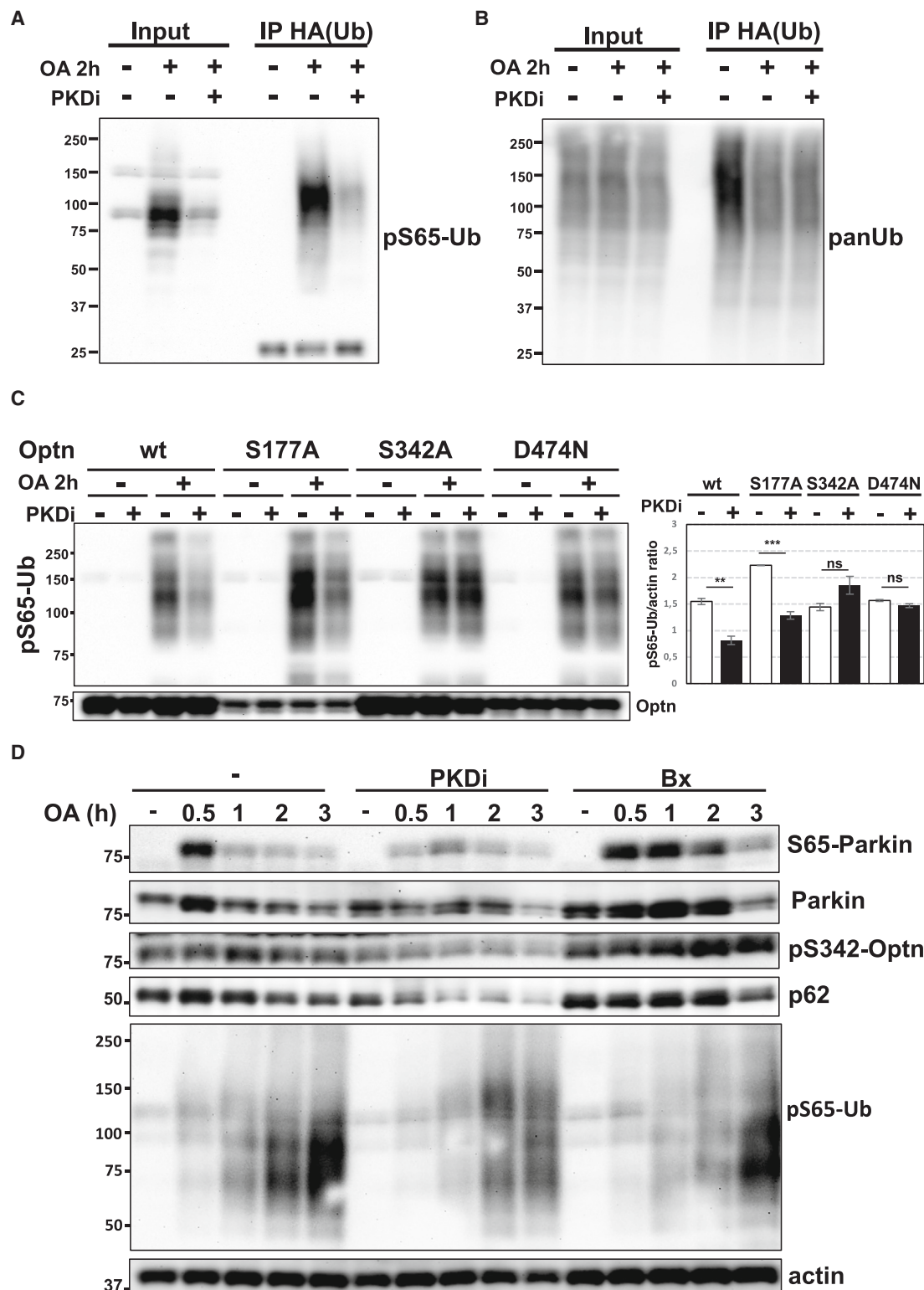
Representative images of Optn-LC3 complexes visualized by *in situ* proximity ligation assays (PLA) during mitophagy are shown. HeLa cells expressing BFP-Parkin were pretreated with PKDi or left untreated as indicated and induced with OA for 4 and 8 h. Images were acquired using a confocal spinning-disk microscope. Bars = 10 μ m. Analyses were conducted on five images from two independent experiments, each containing 10–15 cells identified by the detection of actin protein using Alexa Fluor 488 Phalloidin. The number of Optn-LC3 PLA dots per cell was determined using Cell Profiler software,²³ and statistical significance was determined. Data are represented as boxplot. n.s., not significant. * $p < 0.05$, ** $p < 0.01$, *** $p < 0.001$ (PKDi $n = 59$ vs. NI $n = 71$: $\Delta = -0.494$, $t = -0.315$, $ddl = 117$, $p = 1.000$; PKDi+OA4h $n = 32$ vs. OA4h $n = 47$: $\Delta = -11.0$, $t = -3.90$, $ddl = 68.0$, $p = 0.003$; PKDi+OA8h $n = 53$ vs. OA8h $n = 38$: $\Delta = -13.83$, $t = -3.96$, $ddl = 87.6$, $p = 0.002$).

LC3/GABARAP proteins.¹⁰ Upon mitophagy induction, the number of Optn-LC3 complexes per cell increases after 4 and 8 h (Figure 5A left panels and graph below). Our experiments show that Optn-LC3 complexes are not confined to aggregated mitochondria but distributed throughout the cells, even after mitophagy induction. This localization likely reflects the dispersion of LC3 and Optn proteins in cells, where only a fraction of the LC3-Optn complexes is located to mitochondria. Strikingly, PKD inhibitor treatment resulted in a higher number of Optn-LC3 PLA dots/cell after 4 and 8h of OA induction (Figure 5A right panels and graph below). This increase suggests that activation

of the PKD-Optn pathway hinders the interaction between Optn and LC3.

PKD-mediated phosphorylation of Optn enhances Parkin activity during mitophagy

We next examined whether Optn phosphorylation by PKD could regulate Parkin activity by monitoring S65-phosphorylated ubiquitin, a hallmark of Parkin activity during mitophagy.^{24,25} The pS65-Ub signals were strongly detected after mitophagy induction, but dramatically reduced in the presence of PKDi, both in whole cell lysates and following immunoprecipitation of

**Figure 6. Inhibition of PKD kinases affects Parkin activity**

(A and B) HeLa cells stably expressing Parkin and transiently expressing HA-Ubiquitin were treated with OA, following 45 min pretreatment with PKDi as indicated, and lysed. Ubiquitin-modified complexes were immunoprecipitated from lysate. Immunoprecipitates and Input (total lysate) were resolved on SDS-PAGE and analyzed by Western blot using specific anti-pS65 Ub antibodies (A) or anti-panUb antibodies (B).

(legend continued on next page)

overexpressed HA-tagged ubiquitin, ensuring specificity of the detected signal (**Figure 6A**). In contrast, signal from pan-ubiquitin antibodies was not enhanced by OA and not affected by PKDi (**Figure 6B**). The inhibitory effect of PKDi on pS65-Ub was specifically prevented by S342D or S342A mutation, but not by S177A (**Figures 6C, S6A** and **S6B** for control). The D474N mutation that alters the Ub-binding activity of Optn only marginally affects pS65-Ub signals compared to Optn wt (**Figure 6C**). Subsequently, we conducted western blot on enriched mitochondrial fraction and observed a substantial reduction in the pS65-Ub signal detected in this fraction, when cells were pre-treated with PKDi and induced by OA (**Figure S6C**). Specificity was controlled using the pan-ubiquitin antibodies (**Figure S6C**) and the efficiency of mitochondrial fractionation was validated through the detection of mitochondria-specific proteins such as Mfn-2, PINK1, VDAC-1, and TOM-20 (**Figure S6D**). To assess whether the observed pS65-Ub decrease could be related to higher Parkin degradation rate by autophagy, HeLa-Parkin cells were pretreated with bafilomycin, alone or together with PKDi (**Figures S7A** and **S7B** from two independent experiments). Bafilomycin did not block the inhibition of phospho-S65-Ub by PKDi and had no impact on the expression levels of Parkin, despite its ability to prevent p62 degradation. These findings indicate that Parkin is not degraded in the time course of mitophagy induction used, and that decreased Parkin activity appears to be responsible for the reduction in pS65-Ub levels upon inhibition of PKD activity. Furthermore, bafilomycin co-treatment resulted in significantly lower pS65-Ub levels compared to conditions with the PKD inhibitor alone, suggesting that bafilomycin may further reduce the pS65-Ub levels by inhibiting the autophagy-mediated degradation of a protein that antagonizes Parkin activity, such as a deubiquitinase.

The impact of PKD inhibition on Parkin activity was examined by Western blot over different time points of mitophagy using phosphorylated S65-Parkin antibodies. Compared to control cells in which S65 phosphorylation was detected between 30 min and 1h after induction, PKDi treatment resulted in a decreased S65-Parkin signal (**Figures 6D** and **S8A**). Degradation of p62 that starts after 2 h of induction, was used to monitor the ongoing mitophagy. As expected, PKDi prevented pS342 phosphorylation of Optn, but surprisingly, enhanced p62 degradation, suggesting increased mitophagy efficiency. In contrast to PKDi, cells co-treated with the TBK1 inhibitor exhibited either no effect or sustained S65 phosphorylation of Parkin, along with increased S342 phosphorylation of Optn and reduced p62 degradation, indicating reduced mitophagy efficiency (**Figures 6D** and **S8A**). As previously shown in **Figure 6A** and **6C**, phosphorylated S65-Ub, induced over time, was strongly reduced in the presence of PKDi, but not Bx795

(**Figure 6D**). The effect of PKD on the levels of S65-phosphorylated Parkin and pS65-Ub was further confirmed (although less pronounced) using siRNA targeting PKD kinases and TBK1 expression (**Figures S8B** and **S6E** for control). Importantly, PINK1 expression - the kinase responsible for phosphorylating both S65-Parkin and S65-Ub - remained unaffected by PKDi pre-treatment prior to OA stimulation (**Figure S8C**). In agreement with the results obtained in HeLa cells overexpressing Parkin, inhibition of PKD activity in SH-SY5Y cells, a human neuroblastoma cell line that express endogenous levels of Parkin and Optn,²⁶ resulted in dramatic reduction of the pS65-Ub signals compared to conditions where PKD activity remained active (**Figure S8D**).

PKD inhibition increases mitophagy efficiency

Altogether, our results indicate that PKD inhibition leads to a decrease in Parkin activity and an increase in the interaction between Optn and LC3, suggesting opposing effects on mitophagy. To monitor the resulting effect of PKD activity on the progression of mitophagy, we used the mitochondrial Keima approach that measures the percentage of cells where mitochondria undergo engulfment within autolysosomes, indicative of an acidic environment.²⁷ HeLa cells stably expressing both mitochondrial-targeted Keima and eBFP-Parkin displayed the characteristic wavelength shift upon stimulation of cells with the respiratory chain decoupler, OA or CCCP (**Figure S9A**). Substantial increase (almost 20% after 3 h of OA) in the percentage of cells displaying acidic mitochondria (Keima 561nm positive cells) was observed following PKDi treatment (**Figure 7A**), while treatment with the TBK1 inhibitor (Bx795) nearly abrogated mitophagy induction, consistent with previous observations.¹² Consistently, inhibition of PKD1, 2, and 3 expression by siRNA led to a 15% increase in the fraction of cells undergoing mitophagy after OA treatment (**Figures 7B** and **S6E** for control), confirming the involvement of PKD kinases in the mitophagy process. Conversely, cells lacking TBK1 expression displayed diminished efficiency in OA-induced mitophagy and impaired degradation of p62 (**Figures 7B** and **S6E**). As expected, the effect of PKDi was reversed using bafilomycin which inhibits the autolysosomal acidification (**Figure S9B**). To provide additional validation regarding the specificity of PKD inhibition in inducing mitophagy, we used another PKD inhibitor, namely CRT0066101 (referred thereafter as CRT). Our findings revealed a mitophagy-inducing activity similar to that observed with PKDi, further supporting the targeted effect of PKD inhibition on mitophagy (**Figure S9C**).

Subsequently, we investigated whether the effect of PKD kinases on mitophagy is linked to their ability to phosphorylate Optn. Overexpression of wild-type Optn substantially raised the

(C) HeLa cells overexpressing Parkin and transiently transfected with VSV-tagged Optn wt or its S177A, S342A or D474N mutated forms were treated with PKD and/or OA and lysed. Total lysate was analyzed by Western blot using anti-pS65 Ub and Optn antibodies. Phosphorylated S65-Ubiquitin levels were quantified in stimulated conditions (OA 2h) from 2 independent western blot experiments and depicted in the adjacent graph as the ratio of phosphorylated-S65Ub to actin protein levels presented in **Figure S5B**. Data are represented as average +/- standard deviation. n.s., not significant. * $p < 0.05$, ** $p < 0.01$, *** $p < 0.001$ (WT: OA + PKDi vs. OA $n = 2$, $\Delta = 0.734$, $t = 6.63$, ddl = 8.00, $p = 0.002$; S177A: OA + PKDi vs. OA $n = 2$, $\Delta = 0.946$, $t = 8.54$, ddl = 8.00, $p < 0.001$; S342A: OA + PKDi vs. OA $n = 2$, $\Delta = -0.411$, $t = -3.71$, ddl = 8.00, $p = 0.069$; D474N: OA + PKDi vs. OA $n = 2$, $\Delta = 0.0973$, $t = 0.879$, ddl = 8.00, $p = 0.980$).

(D) Total lysates from HeLa cells overexpressing Parkin pre-treated with PKDi or BX795 (Bx, TBK1 inhibitor) and harvested at different time after mitophagy induction were analyzed by Western blot using anti-pS65 Parkin, Parkin, pS342 Optn, p62, S65-Ub and Actin antibodies.

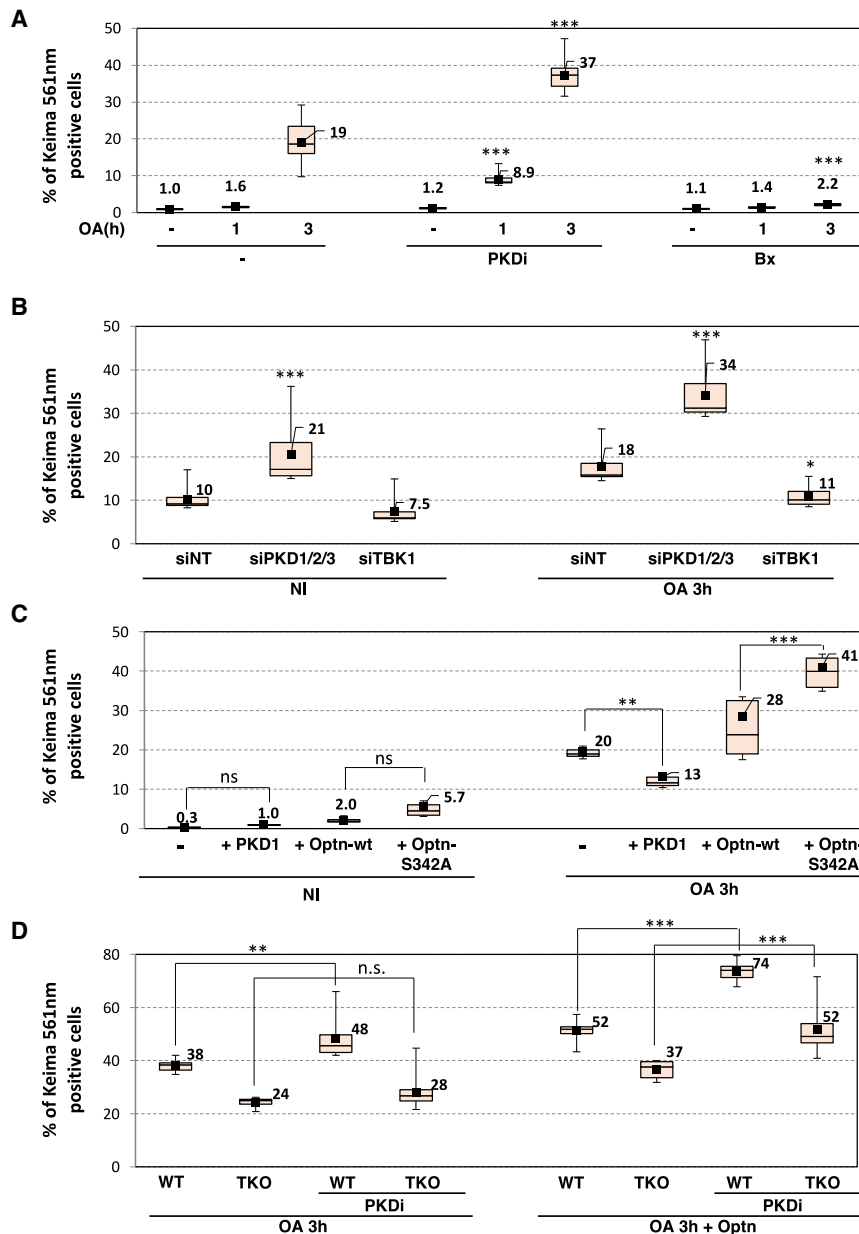


Figure 7. Protein kinase D inhibition affects mitophagy

(A) HeLa cells expressing mitochondria-targeted Keima and BFP-Parkin were pre-treated for 45 min with PKDi or BX795 (Bx) before induction with OA for 1 and 3 h. The analysis was conducted by flow cytometry, and the percentages of cells positive for Keima 561nm (pH4) are showcased using a boxplot graph. Statistical analyses were conducted on 9 independent replicates. * $p < 0.05$, ** $p < 0.01$, *** $p < 0.001$ (PKDi vs. untreated: 1h $n = 9$, $\Delta = -7.32$, $t = -6.00$, ddl = 73.0, $p < 0.001$; 3h $n = 9$, $\Delta = -18.3$, $t = -15.0$, ddl = 73.0, $p < 0.001$; Bx vs. untreated: 1h $n = 9$, $\Delta = 0.182$, $t = 0.149$, ddl = 73.0, $p = 1.000$; 3h $n = 9$, $\Delta = 16.796$, $t = 13.779$, ddl = 73.0, $p < 0.001$).

(B) HeLa cells expressing mitochondria-targeted Keima and BFP-Parkin were transfected with control siRNA (siNT) or siRNA directed against the three isoforms of PKD (siPKD1/2/3) or TBK1 and left 72h before the 3 h induction with OA. The analysis was conducted via flow cytometry, and the percentages of cells positive for Keima 561nm (pH4) are showcased using a boxplot graph. Statistical analyses were conducted on 8 independent replicates. * $p < 0.05$, ** $p < 0.01$, *** $p < 0.001$ (siPKD vs. siNT: NI $n = 8$, $\Delta = -10.2$, $t = -4.49$, ddl = 42.0 $p < 0.001$; OA $n = 8$, $\Delta = -16.4$, $t = -7.17$, ddl = 42.0, $p < 0.001$; siTBK vs. siNT: NI $n = 8$, $\Delta = 2.88$, $t = 1.26$, ddl = 42.0, $p = 0.804$; OA $n = 8$, $\Delta = 8.007$, $t = 3.508$, ddl = 42.0, $p = 0.013$).

(C) HeLa cells expressing mitochondria-targeted Keima, BFP-Parkin with either VSV-tagged Optn wt, Optn-S342A or PKD1 were harvested before and after stimulation by OA. The analysis was conducted by flow cytometry, and the percentages of cells positive for Keima 561nm (pH4) are showcased using a boxplot graph. Statistical analyses were conducted on 8 independent replicates.

n.s. not significant * $p < 0.05$, ** $p < 0.01$, *** $p < 0.001$ (PKDi vs. untreated: NI $n = 8$, $\Delta = -0.716$, $t = -0.377$, ddl = 56.0 $p = 1.000$; OA $n = 8$, $\Delta = 7.71$, $t = -4.06$, ddl = 56.0, $p = 0.004$; S342A vs. WT: NI $n = 8$, $\Delta = -2.67$, $t = -1.41$, ddl = 56.0, $p = 0.851$; OA $n = 8$, $\Delta = -14.2$, $t = -7.49$, ddl = 56.0, $p < 0.001$).

(D) Parental and triple knock-out (TKO, deficient for Optn, NDP52 and Tax1BP1) HeLa cells both expressing BFP-Parkin and mtKeima were transfected with Optn wt and pre-treated for 45 min

with PKDi before induction by OA as indicated. The analysis was conducted by flow cytometry, and the percentages of cells positive for Keima 561nm (pH4) are showcased using a boxplot graph. Statistical analyses were conducted on 10 independent replicates. n.s. not significant * $p < 0.05$, ** $p < 0.01$, *** $p < 0.001$ (WT-PKD1 vs. WT: OA $n = 10$, $\Delta = -10.0$, $t = -4.19$, ddl = 72.0 $p = 0.002$; OA + Optn $n = 22.0$, $\Delta = 7.71$, $t = -9.18$, ddl = 72.0, $p < 0.001$; TKO-PKD1 vs. TKO: OA $n = 10$, $\Delta = -3.67$, $t = -1.53$, ddl = 72.0, $p = 0.786$; OA + Optn $n = 10$, $\Delta = -15.08$, $t = -6.3038$, ddl = 72.0, $p < 0.001$).

percentage of cells with mitochondria at pH4 (from 20 to 28%), that was further increased to 41% following PKD-deficient mutant (Optn-S342A) expression (Figure 7C). In parallel, overexpression of PKD1 strongly decreased this level from 20 to 13% (Figure 7C). To validate the specific role of Optn on PKD-induced mitophagy, we restored expression of Optn wt or expressed different Optn mutants in HeLa-TKO cells stably transfected with mtKeima and eBFP-Parkin (Figures 7D and S9D). Treatment with the PKD inhibitor led to a 38 to 48% enhancement in parental HeLa cells (WT), but failed to elicit a similar increase (24–28%) in

TKO cells (Figure 7D). As anticipated, complementation by Optn wt restored this enhancement (37–52%) in TKO cells. In the same cell context, we showed that Optn-S342A augmented mitophagy (39–50% compared to wild-type Optn) and Optn-S342D expression reduced percentage of cells with acidic mitochondria from 39 to 21% (Figure S9D). As previously established,⁸ Optn S177A mutant expression reduced mitophagy efficiency (down to 22% compared to WT), while TBK1 phosphomimetic mutant S177D increased it up to 51%. Consistent with the necessity of its Ub binding activity, expression of an Ub binding-deficient

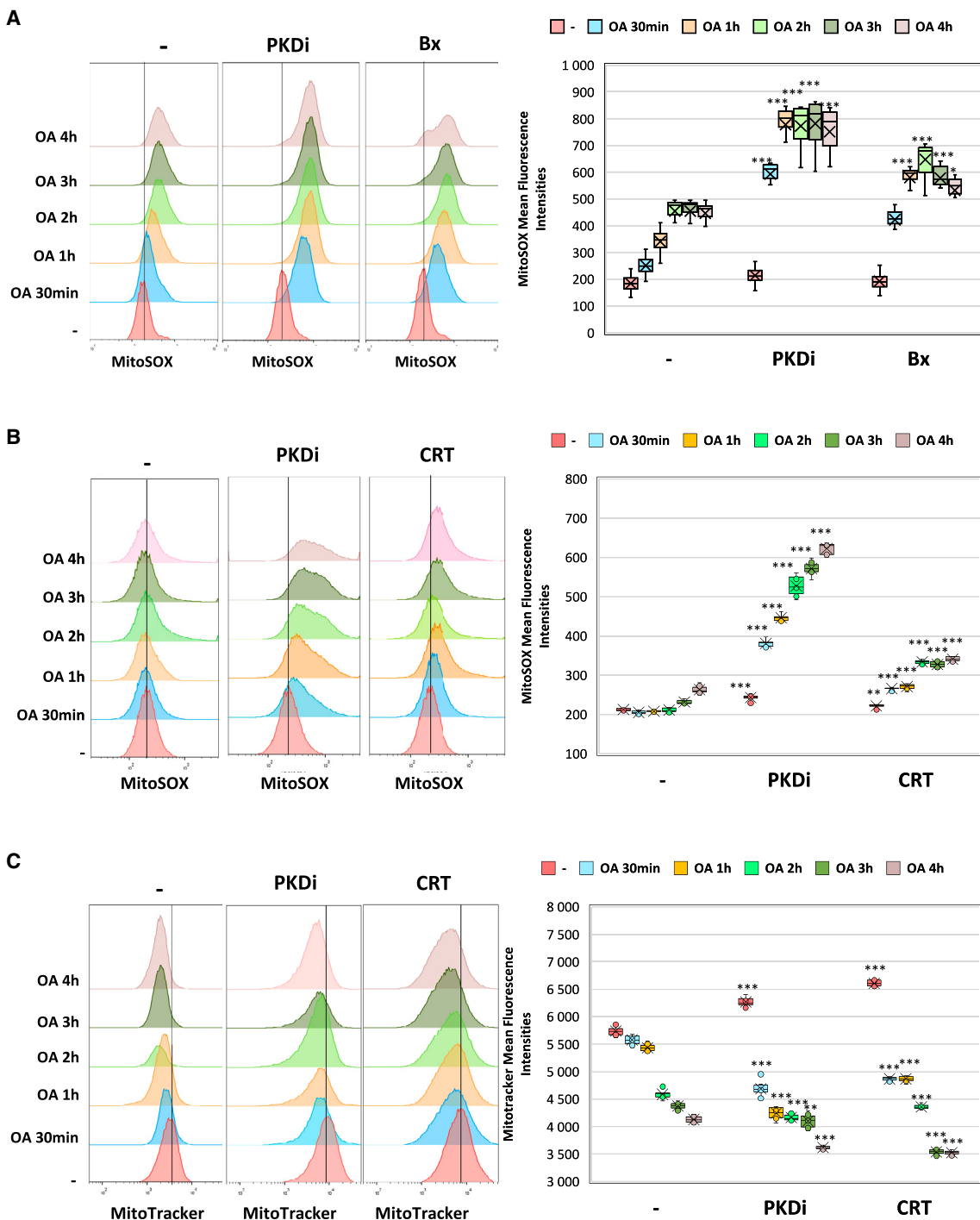


Figure 8. PKD inhibition enhances mitochondrial ROS production and reduces the global mitochondrial mass

(A) Measurement of mitochondrial ROS production in HeLa cells expressing BFP-Parkin, pretreated with PKDi or Bx (Bx795) and induced with OA as indicated. Cells were incubated with 500 nM MitoSOX for 30 min and subjected to cytometry analysis. Quantification of MitoSOX fluorescence was performed in gated positive Parkin expressing cells by cytometry and data analyzed using FlowJo. Data are represented as boxplot. Statistical analyses were conducted on 9 independent replicates. * $p < 0.05$, ** $p < 0.01$, *** $p < 0.001$ (PKDi: $n = 9$ NI: $\Delta = -29.7$, $t = -1.90$, $ddl = 16.0$, $p = 0.877$; OA30min: $\Delta = -343$, $t = -16.82$, $ddl = 15.0$, $p < 0.001$; OA1h: $\Delta = -436$, $t = -15.11$, $ddl = 13.4$, $p < 0.001$; OA2h: $\Delta = -317.56$, $t = -10.274$, $ddl = 12.8$, $p < 0.001$; OA3h: $\Delta = -326.89$, $t = -9.731$, $ddl = 12.4$, $p < 0.001$; OA4h: $\Delta = -305.1$, $t = -9.290$, $ddl = 12.3$, $p < 0.001$; Bx: $n = 9$ NI: $\Delta = -7.89$, $t = -496$, $ddl = 16.0$, $p = 1.000$; OA30min: $\Delta = -171.6$, $t = -9.03$, $ddl = 15.7$, $p < 0.001$; OA1h: $\Delta = -239$, $t = -10.665$, $ddl = 15.9$, $p < 0.001$; OA2h: $\Delta = -193.1$, $t = -7.21$, $ddl = 14.4$, $p < 0.001$; OA3h: $\Delta = -123.00$, $t = -4.7121$, $ddl = 15.2$, $p = 0.018$; OA4h: $\Delta = -84.8$, $t = -3.15$, $ddl = 14.4$, $p = 0.250$).

(legend continued on next page)

mutant of Optn (D474N) markedly impeded mitophagy efficiency (Figure S9D). Altogether, our results indicate that PKD phosphorylation of Optn results in a reduced amount of mitochondria within the acidic autolysosome environment, which contrasts with the effect of TBK1 on mitophagy.

PKD inhibition affects the mitochondrial mass and mROS production

To assess the effect of PKD inhibition on the mitochondrial membrane potential, the global mitochondrial mass levels and the mitochondrial reactive oxygen species (mROS) levels, we performed FACS analyses of Parkin-expressing HeLa cells using tetramethylrhodamine methyl ester perchlorate (TMRM), MitoTracker Red CMXRos and MitoSOX, respectively (Figures 8A, S10A and S10B). Induction of mitophagy by OA led to a decrease of the TMRM intensities that reflects the already known effect of respiratory chain decoupler (especially oligomycin) on the mitochondrial membrane potential (Figure S10A). The TMRM signal was slightly enhanced by PKDi alone, and was not significantly altered by OA co-treatment. In contrast, pre-treatment of cells with TBK1 inhibitor before induction by OA led to a dramatic decrease of TMRM levels, as previously reported in the presence of Parkin.²⁸ Regarding the MitoTracker signal, PKDi treatment led to a substantial reduction in global mitochondrial mass when mitophagy was induced, a phenomenon not observed with OA alone or when TBK1 was inhibited (Figure S10B). We next used the MitoSOX reagent to measure the mROS levels resulting from mitochondrial damages (Figure 8A). Stimulating cells with OA for up to 4 h resulted in a progressive accumulation of mROS, as previously shown.²⁹ Strikingly, treatment with PKDi and OA led to a higher and more rapid increase in mROS. Paradoxically, inhibiting the mitophagy process with Bx795 also amplified mROS, as previously described.^{30,31} Similar results were obtained in the SHSY5Y cells expressing endogenously Parkin, since PKDi or CRT treatment strongly increased the mitochondrial ROS production and reduced the mitochondrial mass after mitophagy induction compared to conditions where PKD activity remained active (Figures 8B and 8C). Altogether, these findings argue for increased mitophagy, marked by higher ROS levels and lower mitochondrial mass, when PKD activity is suppressed, suggesting a notable decline in mitophagy effectiveness upon activation of the PKD-Optn pathway.

Mitochondrial membrane potential (B) and total mitochondria mass (C) were measured in SHSY5Y cells pre-treated with PKDi or CRT and harvested at different time after stimulation with OA as indicated. Cells were incubated with MitoTracker Green FM or MitoSOX for 30 min before FACS analysis. Quantification of the TRMR and MitoTracker signals was performed by flow cytometry, and the Mean Fluorescent Intensities (MFI) of MitoTracker and MitoSOX are showcased using a boxplot graph. Statistical analyses were conducted on 6 independent experiments by performing a pairwise comparison of the same time points of mitophagy induction in the presence or absence of PKDi or CRT. Data are represented as boxplot. MitoTracker MFI * $p < 0.05$, ** $p < 0.01$, *** $p < 0.001$ (PKDi: $n = 9$ NI: $\Delta = -30.6$, $t = -0.866$, $ddl = 18.0$, $p = 1.000$; AO 30min: $\Delta = 888$, $t = 18.75$, $ddl = 15.4$, $p < 0.001$; AO 1h: $\Delta = 1188$, $t = 31.40$, $ddl = 14.9$, $p < 0.001$; AO 2h: $\Delta = 422.0$, $t = 15.49$, $ddl = 17.2$, $p < 0.001$; AO 3h: $\Delta = 273.3$, $t = 6.567$, $ddl = 13.0$, $p < 0.001$; OA 4h: $\Delta = 510$, $t = 25.6$, $ddl = 12.69$, $p < 0.001$; CRT: $n = 9$ NI: $\Delta = -373$, $t = -12.5$, $ddl = 16.2$, $p < 0.001$; OA 30min: $\Delta = 709$, $t = 26.1$, $ddl = 11.17$, $p < 0.001$; OA 1h: $\Delta = 568$, $t = 23.0$, $ddl = 16.82$, $p < 0.001$; OA 2h: $\Delta = 228.9$, $t = 9.142$, $ddl = 15.08$, $p < 0.001$; OA 3h: $\Delta = 835$, $t = 35.9$, $ddl = 17.16$, $p < 0.001$. OA 4h: $\Delta = 608.4$, $t = 27.676$, $ddl = 15.97$, $p < 0.001$; MitoSOX MFI * $p < 0.05$, ** $p < 0.01$, *** $p < 0.001$ (PKDi: $n = 9$ NI: $\Delta = -30.8$, $t = -13.00$, $ddl = 10.33$, $p < 0.001$; AO 30min: $\Delta = -176$, $t = -56.8$, $ddl = 11.89$, $p < 0.001$; AO 1h: $\Delta = -237.8$, $t = -91.4$, $ddl = 13.27$, $p < 0.001$; AO 2h: $\Delta = -316.2$, $t = -39.87$, $ddl = 8.62$, $p < 0.001$; AO 3h: $\Delta = -339.9$, $t = -61.80$, $ddl = 9.38$, $p < 0.001$; AO 4h: $\Delta = -359.2$, $t = -65.63$, $ddl = 14.45$, $p < 0.001$; CRT: $n = 9$ NI: $\Delta = -9.56$, $t = -5.94$, $ddl = 13.41$, $p = 0.003$; OA 30min: $\Delta = -60.67$, $t = -36.002$, $ddl = 13.94$, $p < 0.001$; OA 1h: $\Delta = -62.33$, $t = -27.28$, $ddl = 9.58$, $p < 0.001$; OA 2h: $\Delta = -122.3$, $t = -58.6$, $ddl = 15.89$, $p < 0.001$; OA 3h: $\Delta = -95.11$, $t = -31.45$, $ddl = 13.08$, $p < 0.001$. AO 4h: $\Delta = -77.78$, $t = -21.37$, $ddl = 12.59$, $p < 0.001$).

PKD inhibition enhances Parkin recruitment to damaged mitochondria

The decreased mitophagy observed when PKD is inhibited, however, appears in contradiction with the lower Parkin activity observed in this case. We therefore conducted live cell imaging with HeLa cells expressing exogenously stable Parkin and endogenous Optn to track the recruitment of Parkin to damaged mitochondria, a critical step in the mitophagy process. Results from five independent experiments (Figure 9A and videos in supplemental material) unveiled a more robust and faster recruitment of Parkin onto damaged mitochondria, observed as early as 30 min, when PKD activity is inhibited (OA + PKDi), in contrast to conditions where PKD is activated (OA). These data are consistent with the increased efficiency of mitophagy observed with PKD inhibitors. Colocalization analyses using Pearson correlation confirm the negative regulatory role of PKD in the recruitment of Parkin during mitophagy (Figure 9A and graph below). Same experiments performed in HeLa TKO cells reconstituted with Optn wt demonstrated that the enhancement of Parkin recruitment to mitochondria by PKDi was dependent on Optn re-expression (Figure S11 and graph below). Similar results were obtained in SHSY5Y cells stably expressing a mitochondrial marker, even though endogenous Parkin signal was more diffuse than when overexpressed (Figure S12 and graph below). Again, a robust and earlier recruitment of Parkin onto damaged mitochondria, was observed when PKD activity was inhibited by either PKDi or CRT, in contrast to conditions where PKD was activated. In overall, PKD activation during mitophagy leads to higher Parkin activity, but inhibits mitophagy and rather restricts Parkin recruitment to mitochondria.

DISCUSSION

In this study, we identified PKD family kinases as new effectors of the autophagy receptor function of Optn, providing new steps in the regulation of Parkin-dependent mitophagy. Following the identification of TBK1 as an effector kinase of Optn-mediated autophagy,¹¹ our investigation reports the identification of a family of kinases capable of modulating Optn function in the context of mitophagy. Prior research has indicated that the recruitment of TBK1 to mitochondria and its subsequent activation hinge upon the interaction between Optn and poly-Ub chains.¹¹ Activated TBK1 phosphorylates Optn on Ser473 to stabilize its

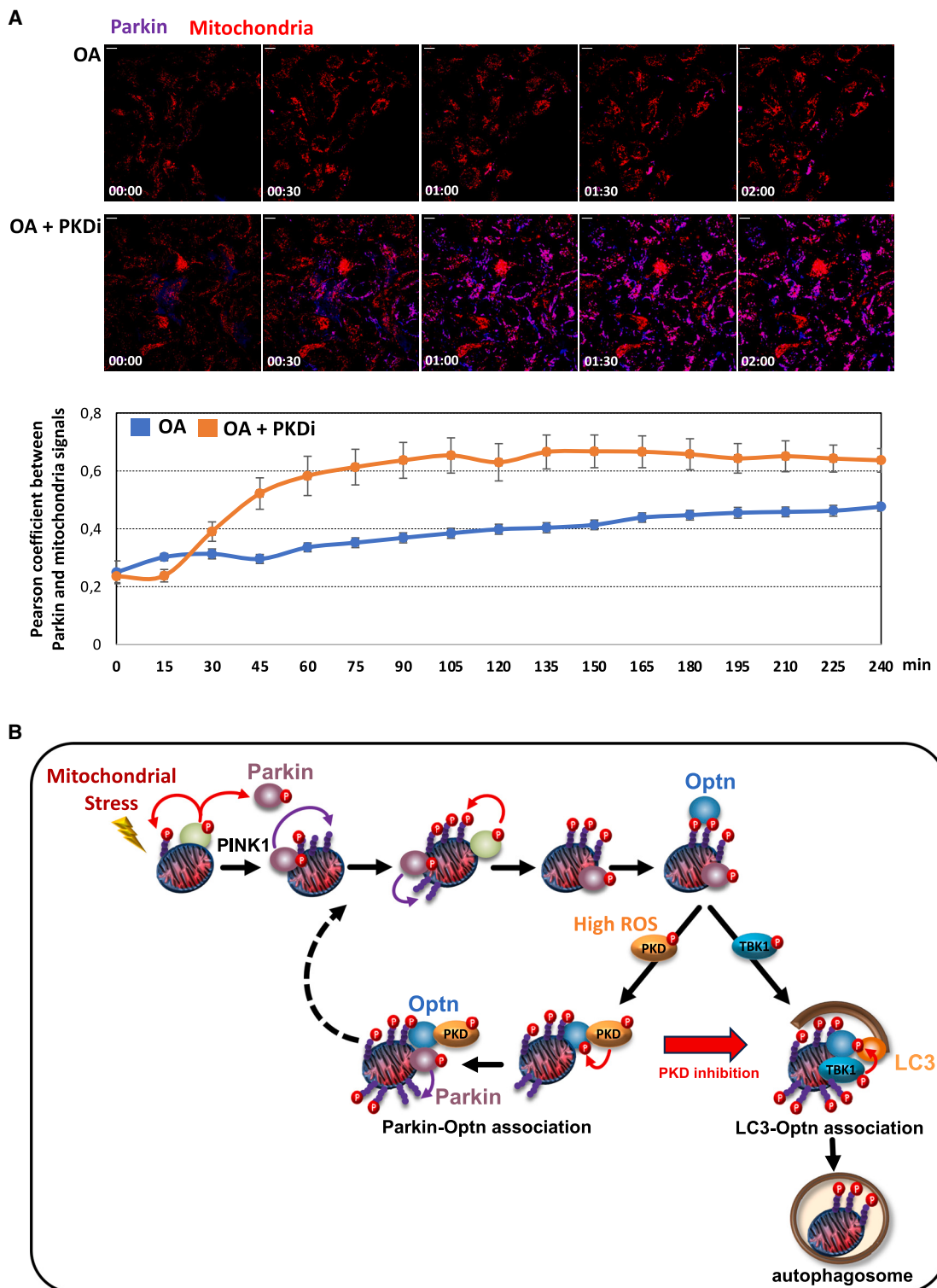


Figure 9. PKD inhibition enhances Parkin recruitment to damaged mitochondria

(A) Live imaging microscopy experiments were conducted using HeLa cells expressing BFP-Parkin and mitochondrial Keima (red signal). Representative images were captured every 30 min for up to 2 h in the absence or presence of a PKD inhibitor. Images were acquired every 15 min over a total of 4 h using a confocal spinning-disk microscope outfitted with a 100x objective lens. Bars = 10 μ m. Parkin recruitment to damaged mitochondria was quantified by calculating the

(legend continued on next page)

binding to various poly-Ub chains and on Ser177 to promote its association with the microtubule-associated protein 1A/1B light chain 3 (LC3).¹¹ In this study, we demonstrate, for the first time, that following mitochondrial depolarization, Protein Kinases D are activated and recruited to mitochondria where they phosphorylate the S342 residue of the LERKNS sequence of Optn. Significantly, this phosphorylation site of Optn has been described as the most frequently referenced modification of Optn in high-throughput studies (<https://www.phosphosite.org/proteinAction.action?id=7793&showAllSites=true>). We found that this phosphorylation event facilitates the previously unreported association between Parkin and Optn. Formation of these complexes in turn increases Parkin activity and consequently the levels of phosphorylated Ub at the mitochondria surface. Strikingly, we found that PKD activation reduces the recruitment of Parkin to mitochondria, consistent with its inhibitory effect on mitophagy. Notably, we observed that the Optn-Parkin complexes are not only localized to damaged mitochondria but are also dispersed throughout the cytoplasm. This suggests that the formation of these complexes might sequester Parkin away from damaged mitochondria, thereby reducing the overall Parkin recruitment. We also showed that inhibition of PKD activities or knockdown of their expression reduces the levels of phosphorylated S65-Parkin and S65-Ub indicating that PKD specifically regulates the phosphorylated ubiquitin levels of mitochondrial proteins, but not their overall ubiquitination. However, treatment with a PKD inhibitor does not impact PINK1 accumulation on the mitochondrial surface, which is required for Ser65-Ub and Ser65-Parkin phosphorylation. Using phosphodeficient and phosphomimetic mutant of Optn, we further demonstrated that this effect is dependent on Optn phosphorylation by PKD.

An important issue lies in understanding how the phosphorylation of Optn by PKD can regulate Parkin activity that was reported to be enhanced by phosphorylation of its ubiquitin like (UBL) domain or by binding to pSer65-Ub.^{32,33} Given that both phosphorylation events were augmented by PKD activation, local accumulation of Parkin induced by the association of Parkin and Optn might stimulate PINK1 activity, by increasing its interaction with Parkin.³⁴ Indirectly, accumulation of pSer65-Ub (20% of the Ub molecules) on damaged mitochondria promotes the recruitment of cytosolic unphosphorylated Parkin, but also favors retention on mitochondria of pSer65-Parkin that can in turn provides additional ubiquitin molecules for phosphorylation by PINK1, creating a feedforward mechanism.³² In our model, activation of the PKD kinases can serve as an additional mechanism to enhance Parkin activity through

their ability to favor Parkin-Optn complexes (Figure 9B). Imaging studies have shown that pSer65-Ub signals uniformly coat damaged mitochondria, whereas mitophagy receptors are recruited to highly focal puncta on the surface of mitochondria.⁸ The Parkin-Optn complexes could therefore localize to these focal points (and not all over the mitochondria), allowing ubiquitination of yet unmodified surrounding proteins. In turn, the newly ubiquitinated mitochondrial proteins could serve as docking sites for recruitment of other Optn-Parkin complexes, amplifying the ubiquitination signals at mitochondria surface. Such amplification step could be ended by the PINK-mediated Ub phosphorylation, since it was shown that Optn (as well as NDP52 and p62) binds efficiently to unphosphorylated ubiquitin chains, and that their binding is abolished following Ub phosphorylation on Ser65.³⁵ Finally, formation of the Optn-Parkin complex might hinder the phosphorylation of Optn by TBK1 on S177, which is responsible for Optn's interaction with LC3. This inference is supported by the observation that Optn-LC3 complex formation increases when PKD activity is inhibited. Notably, it has been reported that Parkin can interact with TBK1, promoting TBK1 auto-phosphorylation activation through K63-linked ubiquitination modification.²⁸ Overall, these findings suggest a potential competition between the PKD and TBK1 pathways: Parkin's binding to Optn, regulated by PKD, could impede or delay TBK1 activation by Parkin, subsequent Optn phosphorylation and interaction with LC3. In support of this hypothesis, the interaction domain we mapped between PKD and Optn includes the LC3-interaction region (LIR) domain of Optn, thus offering a mechanistic explanation for this competitive relationship. Unlike p62, we did not observe any degradation of the autophagy receptors Optn and NDP52 during the mitophagy induction time course used in our study, suggesting that it may occur at later time points.

Interestingly, Protein kinase D activation is dependent on the oxidative stress levels which are, in the mitophagy process, mainly driven by mitochondrial ROS produced by damaged mitochondria.^{14,36} Indeed, mitochondria-derived reactive oxygen species (mROS) trigger tyrosine phosphorylation of PKD1 preceding that of Ser-phosphorylation at the activation loop and phosphorylation at tyrosine is required for the docking of PKD1 at the mitochondria.³⁷ In parallel, mROS species induce activation of phospholipase D1 which generates diacylglycerol (DAG) that maintains PKD1 binding to mitochondria.³⁸ It is therefore tempting to speculate that activities of the PKD kinases are gradually engaged as the local mitochondrial ROS levels raised.

Pearson coefficient between Parkin and Keima signals. Quantification was carried out on data collected from five independent experiments for each condition. Data are represented as average \pm standard deviation.

(B) Schematic model of the Optn-dependent mitophagy process. Following mitochondrial stress, PINK1 kinase activates Parkin through phosphorylation (pSer65-Parkin) and also phosphorylates ubiquitin chains (phospho-Ser65-Ubiquitin) on the mitochondrial surface. Accumulation of phospho-Ser65-Ubiquitin on damaged mitochondria can promote retention of pSer65-Parkin that can in turn provides additional ubiquitin molecules for phosphorylation by PINK1, creating a feedforward mechanism. Our data suggest that, when a local mitochondrial ROS threshold is reached, activation of the PKD kinases can enhance Parkin activity through their ability to favor Parkin-Optn complexes. Paradoxically, we found that inhibition of PKD activity leads to higher mitophagy efficiency as depicted by the red arrow. We hypothesize that formation of Optn-Parkin complexes might prevent interaction of Optn and LC3 by steric hindrance (the identified PKD-Optn interaction region encompassing the LIR domain of Optn), leading to reduced or delayed autophagosome formation. Due to the transient nature of PKD-mediated phosphorylation of Optn, disrupting the Optn-Parkin complex over time could promote the interaction between Optn and LC3. Subsequently, TBK1 kinase, activated and recruited during mitophagy induction, increases the affinity of Optn for the autophagosomal marker family members LC3 in order to elongate and mature the autophagosome vesicle, completing the entire mitophagy process.

This leads to increased Parkin phosphorylation, a hallmark of its activity, and consequently higher levels of pS65-ubiquitin. PKD activation may therefore enhance the number of mitochondria targeted for degradation, thereby safeguarding cells against oxidative stress damage. In addition to the mitophagy role we have uncovered, recent research suggests that the direct phosphorylation of mitochondrial fission factor (MFF) by PKD is essential for mitochondrial fission during mitosis, but dispensable during interphase.³⁹ However, the precise subcellular localization of PKD in this context remains unspecified. In cardiomyocytes, PKD kinases are engaged downstream of Gq protein-coupled receptor (GqPCR) activation, translocating from the cytosol to the outer mitochondrial membrane, where they directly phosphorylate dynamin-related protein 1 (DRP1) at serine 637.¹⁷ Consequently, DRP1 associates with the outer mitochondrial membrane, promoting mitochondrial fragmentation, ROS production, and apoptotic signaling. The interplay between these mitochondrial activities and mitophagy warrants further investigation.

The most studied isoform of PKD during oxidative stress is PKD1,¹⁵ but the three PKD isoforms were shown to be activated by oxidative stress, although via different phosphorylation mechanisms. Isoform- and cell-type specific behaviors in oxidative stress have been observed, but lack extensive investigations to decipher isoform-specific roles. HeLa cells, the cellular model used in this study, do not express endogenous Parkin, but display detectable levels of PKD expression using antibodies that recognize the three isoforms of PKD, although HeLa cells were reported to express lower levels of PKD1 compared to PKD2 and PKD3.⁴⁰ The individual roles of the three PKD isoforms in mitophagy require further investigation, even though our study demonstrated that all three PKDs are recruited to damaged mitochondria following mitophagy stimulation.

Parkin and PINK1 have been found to be mutated in neurodegenerative diseases such as Parkinson, and mutations in TBK1 and Optn that affect the TBK1-Optn interaction have been also associated with amyotrophic lateral sclerosis (ALS) and frontal temporal dementia.^{41,42} Furthermore, copy-number variations of *TBK1* gene and missense/gain-of-function (such as E50K) mutations in *Optn* gene, are known to cause high-penetrance, autosomal dominant forms of Normal Tension Glaucoma, another neurodegenerative disease.^{43–45} A major question in this medical research field is to design small molecules that target Parkin activity in order to facilitate the removal of damaged mitochondria. Our findings that treatment of cells with PKD inhibitor increases mitophagy even if Parkin and Ub phosphorylation are reduced, suggest that these compounds could fulfill, at least in part, the expectations for potential therapeutic strategy in neurodegenerative disease such as Glaucoma, Parkinson or ALS. It is well known that mitophagy defaults lead to accumulation of damaged mitochondria and promote carcinogenesis.⁴⁶ At the opposite, functional mitophagy inhibits the accumulation of damaged mitochondria and prevents carcinogenesis. For example, overexpression of Parkin can inhibit the proliferation of colorectal cancer cells.⁴⁷ Therefore, chemical that have the capacity to increase or promote mitophagy should open avenues for cancer treatments.

As PKD family members have been associated with cancer by virtue of their regulating role in cell proliferation, differentiation, programmed cell death migration and invasion,⁴⁸ small-molecule inhibitors of PKD have gain attention as therapeutic potential in various cancer model.^{49,50} Indeed, several specific- or pan-PKD inhibitors have demonstrated *in vitro* and *in vivo* antitumoral activity in diverse cancer scenarios. Despite these effects, no PKD-related inhibitors have currently entered clinical trials likely due to similar or opposite roles of PKD isoforms in different cancers. Our findings that PKD kinases are involved in mitophagy could therefore add a perspective not only for the comprehension of the complex effects of PKD inhibitors on tumor cells, but also as a therapeutic strategy to fight cancer.

Limitations of the study

This research is limited by its use of cell lines rather than primary cells, despite their practical benefits such as efficient transfection and easy knockdown. Indeed, cell lines may not fully replicate the complexity of *in vivo* systems, necessitating validation in physiologically relevant settings like primary cells or animal models. Another constraint arises from the reliance on overexpression studies to explore specific molecular mechanisms. However, overexpression studies in triple knockout HeLa cells were indispensable in deciphering the role of residue phosphorylation of Optn in mitophagy, due to the redundancy of autophagic receptor function in mitophagy as previously noted in Lazarou et al.⁵ Ultimately, knock-in mice expressing mutants of Optn will be essential for fully validating the biological consequences of the PKD-Optn pathway in mitophagy. The use of chemical compounds poses another limitation to this study due to concerns over off-target effects, especially at elevated concentrations. The PKD inhibitor CID2011756 was used at 5µM, a concentration not exceedingly high for a kinase inhibitor and efficiently inhibiting PKD activity (as evidenced by auto/*trans*-phosphorylation status). To mitigate this concern, we employed a multifaceted approach, including use of an alternative PKD inhibitor (CRT0066101) and siRNA method to suppress PKD expression, both confirming the effects observed on the Parkin-dependent mitophagy process. However, effect of PKD inhibitors on signaling pathways beyond PKD cannot be excluded.

RESOURCE AVAILABILITY

Lead contact

Further information and requests for resources and reagents should be directed to and will be fulfilled by the lead contact, P.G. (pierre.genin@sorbonne-universite.fr).

Materials availability

This study did not generate new unique reagents.

Data and code availability

- Data: All raw data reported in this paper will be shared by the [lead contact](#) upon request.
- Code: No code were generated in this study.
- Other items: Any additional information required to reanalyze the data reported in this paper is available from the [lead contact](#) upon request.

ACKNOWLEDGMENTS

We thank Pr. Richard Youle (National Institute of Neurological Disorders and Stroke, NIH, USA) for providing us with the triple knockout (TKO) HeLa cell line (also acknowledging Henrietta Lacks and her family), Pr. Atsushi Miyawaki (RIKEN, Japan) for pMT-mKeima-Red plasmid and Pr. Wei Yuan Yang (Institute of Biochemical Sciences, Taiwan) for the eBFP2-Parkin construct. We also thank former members of the “Signaling and pathogenesis” team and especially Nathalie Petiot for her technical help, as well as those of the CIMI-Paris for helpful discussions. We also thank the flux cytometry platform of the Pasteur Institute and especially Pierre-Henri Commere. P.G., E.L. and R.W. were supported by CNRS. Research was supported by the Institut Pasteur, le Centre Nationale pour la Recherche Scientifique (CNRS), l’Institut National de la Santé et de la Recherche Médicale (INSERM), Sorbonne Université et la Cancéropôle Île-de-France (Emergence 2017–2018).

AUTHOR CONTRIBUTIONS

P.G., E.L., and R.W. conceived of and designed the study. E.L. performed the PKD-Optn phosphorylation and interaction studies. P.G., M.A., A.O., S.C., A.Y., and E.B. performed all other experiments. P.G., M.A., E.L., and R.W. analyzed the data. P.G. and R.W. wrote the manuscript, and all others corrected and contributed to it.

DECLARATION OF INTERESTS

The author declares that the research was conducted in the absence of any commercial or financial relationships that could be construed as a potential conflict of interest.

STAR★METHODS

Detailed methods are provided in the online version of this paper and include the following:

- KEY RESOURCES TABLE
- EXPERIMENTAL MODEL AND STUDY PARTICIPANT DETAILS
- METHOD DETAILS
 - Cells and induction
 - Cell extracts, immunoprecipitations and immunoblots
 - Kinase assay
 - Immunofluorescence and *in situ* proximity ligation assay
 - Measurement of mitophagy efficiency by the mitochondrial-targeted-Keima protein
 - Measurement of the mitophagy process by flow cytometry
 - Live-cell imaging
- QUANTIFICATION AND STATISTICAL ANALYSIS
 - Image processing and statistical analyses
 - Line scans
 - Immunoblotting quantification

SUPPLEMENTAL INFORMATION

Supplemental information can be found online at <https://doi.org/10.1016/j.isci.2024.111384>.

Received: April 17, 2024

Revised: August 1, 2024

Accepted: November 11, 2024

Published: November 13, 2024

REFERENCES

1. Xu, Z., Yang, L., Xu, S., Zhang, Z., and Cao, Y. (2015). The receptor proteins: pivotal roles in selective autophagy. *Acta Biochim. Biophys. Sin.* 47, 571–580. <https://doi.org/10.1093/abbs/gmv055>.
2. Martinez-Vicente, M. (2017). Neuronal Mitophagy in Neurodegenerative Diseases. *Front. Mol. Neurosci.* 10, 64. <https://doi.org/10.3389/fnmol.2017.00064>.
3. Kane, L.A., Lazarou, M., Fogel, A.I., Li, Y., Yamano, K., Sarraf, S.A., Banerjee, S., and Youle, R.J. (2014). PINK1 phosphorylates ubiquitin to activate Parkin E3 ubiquitin ligase activity. *J. Cell Biol.* 205, 143–153. <https://doi.org/10.1083/jcb.201402104>.
4. Nguyen, T.N., Padman, B.S., and Lazarou, M. (2016). Deciphering the Molecular Signals of PINK1/Parkin Mitophagy. *Trends Cell Biol.* 26, 733–744. <https://doi.org/10.1016/j.tcb.2016.05.008>.
5. Lazarou, M., Sliter, D.A., Kane, L.A., Sarraf, S.A., Wang, C., Burman, J.L., Sideris, D.P., Fogel, A.I., and Youle, R.J. (2015). The ubiquitin kinase PINK1 recruits autophagy receptors to induce mitophagy. *Nature* 524, 309–314. <https://doi.org/10.1038/nature14893>.
6. Wong, Y.C., and Holzbaur, E.L.F. (2014). Optineurin is an autophagy receptor for damaged mitochondria in parkin-mediated mitophagy that is disrupted by an ALS-linked mutation. *Proc. Natl. Acad. Sci. USA* 111, E4439–E4448. <https://doi.org/10.1073/pnas.1405752111>.
7. Moore, A.S., and Holzbaur, E.L.F. (2016). Dynamic recruitment and activation of ALS-associated TBK1 with its target optineurin are required for efficient mitophagy. *Proc. Natl. Acad. Sci. USA* 113, E3349–E3358. <https://doi.org/10.1073/pnas.1523810113>.
8. Heo, J.M., Ordureau, A., Paulo, J.A., Rinehart, J., and Harper, J.W. (2015). The PINK1-PARKIN Mitochondrial Ubiquitylation Pathway Drives a Program of OPTN/NDP52 Recruitment and TBK1 Activation to Promote Mitophagy. *Mol. Cell* 60, 7–20. <https://doi.org/10.1016/j.molcel.2015.08.016>.
9. Korac, J., Schaeffer, V., Kovacevic, I., Clement, A.M., Jungblut, B., Behl, C., Terzic, J., and Dikic, I. (2013). Ubiquitin-independent function of optineurin in autophasic clearance of protein aggregates. *J. Cell Sci.* 126, 580–592. <https://doi.org/10.1242/jcs.114926>.
10. Wild, P., Farhan, H., McEwan, D.G., Wagner, S., Rogov, V.V., Brady, N.R., Richter, B., Korac, J., Waidmann, O., Choudhary, C., et al. (2011). Phosphorylation of the autophagy receptor optineurin restricts Salmonella growth. *Science* 333, 228–233. <https://doi.org/10.1126/science.1205405>.
11. Richter, B., Sliter, D.A., Herhaus, L., Stolz, A., Wang, C., Beli, P., Zaffagnini, G., Wild, P., Martens, S., Wagner, S.A., et al. (2016). Phosphorylation of OPTN by TBK1 enhances its binding to Ub chains and promotes selective autophagy of damaged mitochondria. *Proc. Natl. Acad. Sci. USA* 113, 4039–4044. <https://doi.org/10.1073/pnas.1523926113>.
12. Matsumoto, G., Shimogori, T., Hattori, N., and Nukina, N. (2015). TBK1 controls autophagosomal engulfment of polyubiquitinated mitochondria through p62/SQSTM1 phosphorylation. *Hum. Mol. Genet.* 24, 4429–4442. <https://doi.org/10.1093/hmg/ddv179>.
13. Zhang, X., Connelly, J., Chao, Y., and Wang, Q.J. (2021). Multifaceted Functions of Protein Kinase D in Pathological Processes and Human Diseases. *Biomolecules* 11, 483. <https://doi.org/10.3390/biom11030483>.
14. Eisenberg-Lerner, A., and Kimchi, A. (2012). PKD is a kinase of Vps34 that mediates ROS-induced autophagy downstream of DAPk. *Cell Death Differ.* 19, 788–797. <https://doi.org/10.1038/cdd.2011.149>.
15. Cobbaut, M., and Van Lint, J. (2018). Function and Regulation of Protein Kinase D in Oxidative Stress: A Tale of Isoforms. *Oxid. Med. Cell. Longev.* 2018, 2138502. <https://doi.org/10.1155/2018/2138502>.
16. Palikaras, K., and Tavernarakis, N. (2014). Mitochondrial homeostasis: the interplay between mitophagy and mitochondrial biogenesis. *Exp. Gerontol.* 56, 182–188. <https://doi.org/10.1016/j.exger.2014.01.021>.
17. Jhun, B.S., O-Uchi, J., Adaniya, S.M., Mancini, T.J., Cao, J.L., King, M.E., Landi, A.K., Ma, H., Shin, M., Yang, D., et al. (2018). Protein kinase D activation induces mitochondrial fragmentation and dysfunction in cardiomyocytes. *J. Physiol.* 596, 827–855. <https://doi.org/10.1113/JP275418>.
18. Rozengurt, E. (2011). Protein kinase D signaling: multiple biological functions in health and disease. *Physiology* 26, 23–33. <https://doi.org/10.1152/physiol.00037.2010>.

19. Allen, G.F.G., Toth, R., James, J., and Ganley, I.G. (2013). Loss of iron triggers PINK1/Parkin-independent mitophagy. *EMBO Rep.* 14, 1127–1135. <https://doi.org/10.1038/embor.2013.168>.
20. Geisler, S., Holmström, K.M., Skujat, D., Fiesel, F.C., Rothfuss, O.C., Kahle, P.J., and Springer, W. (2010). PINK1/Parkin-mediated mitophagy is dependent on VDAC1 and p62/SQSTM1. *Nat. Cell Biol.* 12, 119–131. <https://doi.org/10.1038/ncb2012>.
21. Lagache, T., Grassart, A., Dallongeville, S., Faklaris, O., Sauvonnet, N., Dufour, A., Danglot, L., and Olivo-Marin, J.C. (2018). Mapping molecular assemblies with fluorescence microscopy and object-based spatial statistics. *Nat. Commun.* 9, 698. <https://doi.org/10.1038/s41467-018-03053-x>.
22. Sharlow, E.R., Mustata Wilson, G., Close, D., Leimgruber, S., Tandon, M., Reed, R.B., Shun, T.Y., Wang, Q.J., Wipf, P., and Lazo, J.S. (2011). Discovery of diverse small molecule chemotypes with cell-based PKD1 inhibitory activity. *PLoS One* 6, e25134. <https://doi.org/10.1371/journal.pone.0025134>.
23. Stirling, D.R., Swain-Bowden, M.J., Lucas, A.M., Carpenter, A.E., Cimini, B.A., and Goodman, A. (2021). CellProfiler 4: improvements in speed, utility and usability. *BMC Bioinf.* 22, 433. <https://doi.org/10.1186/s12859-021-04344-9>.
24. Sarraf, S.A., Raman, M., Guarani-Pereira, V., Sowa, M.E., Huttlin, E.L., Gygi, S.P., and Harper, J.W. (2013). Landscape of the PARKIN-dependent ubiquitylome in response to mitochondrial depolarization. *Nature* 496, 372–376. <https://doi.org/10.1038/nature12043>.
25. Sauve, V., Lilov, A., Seirafi, M., Vranas, M., Rasool, S., Kozlov, G., Sprules, T., Wang, J., Trempe, J.F., and Gehring, K. (2015). A Ubl/ubiquitin switch in the activation of Parkin. *The EMBO journal* 34, 2492–2505. <https://doi.org/10.15225/embj.201592237>.
26. Narendra, D., Tanaka, A., Suen, D.F., and Youle, R.J. (2008). Parkin is recruited selectively to impaired mitochondria and promotes their autophagy. *J. Cell Biol.* 183, 795–803. <https://doi.org/10.1083/jcb.200809125>.
27. Fang, E.F., Palikaras, K., Sun, N., Fivenson, E.M., Spangler, R.D., Kerr, J.S., Cordonnier, S.A., Hou, Y., Dombi, E., Kassahun, H., et al. (2017). In Vitro and In Vivo Detection of Mitophagy in Human Cells, C. Elegans, and Mice. *J. Vis. Exp.* 129, 56301. <https://doi.org/10.3791/56301>.
28. Gao, B., Yu, W., Lv, P., Liang, X., Sun, S., and Zhang, Y. (2021). Parkin overexpression alleviates cardiac aging through facilitating K63-polyubiquitination of TBK1 to facilitate mitophagy. *Biochim. Biophys. Acta, Mol. Basis Dis.* 1867, 165997. <https://doi.org/10.1016/j.bbadiis.2020.165997>.
29. Polster, B.M., Nicholls, D.G., Ge, S.X., and Roelofs, B.A. (2014). Use of potentiometric fluorophores in the measurement of mitochondrial reactive oxygen species. *Methods Enzymol.* 547, 225–250. <https://doi.org/10.1016/B978-0-12-801415-8.00013-8>.
30. Zhou, R., Yazdi, A.S., Menu, P., and Tschoopp, J. (2011). A role for mitochondria in NLRP3 inflammasome activation. *Nature* 469, 221–225. <https://doi.org/10.1038/nature09663>.
31. Patoli, D., Mignotte, F., Deckert, V., Dusuel, A., Dumont, A., Rieu, A., Jalil, A., Van Dongen, K., Bourgeois, T., Gautier, T., et al. (2020). Inhibition of mitophagy drives macrophage activation and antibacterial defense during sepsis. *J. Clin. Invest.* 130, 5858–5874. <https://doi.org/10.1172/JCI130996>.
32. Ordureau, A., Sarraf, S.A., Duda, D.M., Heo, J.M., Jedrychowski, M.P., Sviderskiy, V.O., Olszewski, J.L., Koerber, J.T., Xie, T., Beausoleil, S.A., et al. (2014). Quantitative proteomics reveal a feedforward mechanism for mitochondrial PARKIN translocation and ubiquitin chain synthesis. *Mol. Cell* 56, 360–375. <https://doi.org/10.1016/j.molcel.2014.09.007>.
33. Wauer, T., Simicek, M., Schubert, A., and Komander, D. (2015). Mechanism of phospho-ubiquitin-induced PARKIN activation. *Nature* 524, 370–374. <https://doi.org/10.1038/nature14879>.
34. Lazarou, M., Jin, S.M., Kane, L.A., and Youle, R.J. (2012). Role of PINK1 binding to the TOM complex and alternate intracellular membranes in recruitment and activation of the E3 ligase Parkin. *Dev. Cell* 22, 320–333. <https://doi.org/10.1016/j.devcel.2011.12.014>.
35. Ordureau, A., Heo, J.M., Duda, D.M., Paulo, J.A., Olszewski, J.L., Yanish-evski, D., Rinehart, J., Schulman, B.A., and Harper, J.W. (2015). Defining roles of PARKIN and ubiquitin phosphorylation by PINK1 in mitochondrial quality control using a ubiquitin replacement strategy. *Proc. Natl. Acad. Sci. USA* 112, 6637–6642. <https://doi.org/10.1073/pnas.1506593112>.
36. Schofield, J.H., and Schafer, Z.T. (2021). Mitochondrial Reactive Oxygen Species and Mitophagy: A Complex and Nuanced Relationship. *Antioxid. Redox Signal.* 34, 517–530. <https://doi.org/10.1089/ars.2020.8058>.
37. Wit, M., Belykh, A., and Sumara, G. (2024). Protein kinase D (PKD) on the crossroad of lipid absorption, synthesis and utilization. *Biochim. Biophys. Acta, Mol. Cell Res.* 1871, 119653. <https://doi.org/10.1016/j.bbamcr.2023.119653>.
38. Doppler, H., and Storz, P. (2017). Mitochondrial and Oxidative Stress-Mediated Activation of Protein Kinase D1 and Its Importance in Pancreatic Cancer. *Frontiers in oncology* 7, 41. <https://doi.org/10.3389/fonc.2017.00041>.
39. Pangou, E., Bielska, O., Guerber, L., Schmucker, S., Agote-Arán, A., Ye, T., Liao, Y., Puig-Gamez, M., Grandgirard, E., Kleiss, C., et al. (2021). A PKD-MFF signaling axis couples mitochondrial fission to mitotic progression. *Cell Rep.* 35, 109129. <https://doi.org/10.1016/j.celrep.2021.109129>.
40. Bossard, C., Bresson, D., Polishchuk, R.S., and Malhotra, V. (2007). Dimeric PKD regulates membrane fission to form transport carriers at the TGN. *J. Cell Biol.* 179, 1123–1131. <https://doi.org/10.1083/jcb.200703166>.
41. Freischmidt, A., Wieland, T., Richter, B., Ruf, W., Schaeffer, V., Müller, K., Marroquin, N., Nordin, F., Hübers, A., Weydt, P., et al. (2015). Haploinsufficiency of TBK1 causes familial ALS and fronto-temporal dementia. *Nat. Neurosci.* 18, 631–636. <https://doi.org/10.1038/nn.4000>.
42. Weishaupt, J.H., Waibel, S., Birve, A., Volk, A.E., Mayer, B., Meyer, T., Ludolph, A.C., and Andersen, P.M. (2013). A novel optineurin truncating mutation and three glaucoma-associated missense variants in patients with familial amyotrophic lateral sclerosis in Germany. *Neurobiol. Aging* 34, 1516. <https://doi.org/10.1016/j.neurobiolaging.2012.09.007>.
43. Shim, M.S., Takihara, Y., Kim, K.Y., Iwata, T., Yue, B.Y.J.T., Inatani, M., Weinreb, R.N., Perkins, G.A., and Ju, W.K. (2016). Mitochondrial pathogenic mechanism and degradation in optineurin E50K mutation-mediated retinal ganglion cell degeneration. *Sci. Rep.* 6, 33830. <https://doi.org/10.1038/srep33830>.
44. Awadalla, M.S., Fingert, J.H., Roos, B.E., Chen, S., Holmes, R., Graham, S.L., Chehade, M., Galanopolous, A., Ridge, B., Souzeau, E., et al. (2015). Copy number variations of TBK1 in Australian patients with primary open-angle glaucoma. *Am. J. Ophthalmol.* 159, 124–130.e1. <https://doi.org/10.1016/j.ajo.2014.09.044>.
45. Sirohi, K., and Swarup, G. (2016). Defects in autophagy caused by glaucoma-associated mutations in optineurin. *Exp. Eye Res.* 144, 54–63. <https://doi.org/10.1016/j.exer.2015.08.020>.
46. Guan, Y., Wang, Y., Li, B., Shen, K., Li, Q., Ni, Y., and Huang, L. (2021). Mitophagy in carcinogenesis, drug resistance and anticancer therapeutics. *Cancer Cell Int.* 21, 350. <https://doi.org/10.1186/s12935-021-02065-w>.
47. Poulogiannis, G., McIntrye, R.E., Dimitriadi, M., Apps, J.R., Wilson, C.H., Ichimura, K., Luo, F., Cantley, L.C., Wyllie, A.H., Adams, D.J., and Arends, M.J. (2010). PARK2 deletions occur frequently in sporadic colorectal cancer and accelerate adenoma development in Apc mutant mice. *Proc. Natl. Acad. Sci. USA* 107, 15145–15150. <https://doi.org/10.1073/pnas.1009941107>.
48. Roy, A., Ye, J., Deng, F., and Wang, Q.J. (2017). Protein kinase D signaling in cancer: A friend or foe? *Biochim. Biophys. Acta, Rev. Cancer* 1868, 283–294. <https://doi.org/10.1016/j.bbcan.2017.05.008>.
49. Lv, D., Chen, H., Feng, Y., Cui, B., Kang, Y., Zhang, P., Luo, M., and Chen, J. (2021). Small-Molecule Inhibitor Targeting Protein Kinase D: A Potential

- Therapeutic Strategy. *Front. Oncol.* 11, 680221. <https://doi.org/10.3389/fonc.2021.680221>.
50. Wang, Q.J., and Wipf, P. (2023). Small Molecule Inhibitors of Protein Kinase D: Early Development, Current Approaches, and Future Directions. *J. Med. Chem.* 66, 122–139. <https://doi.org/10.1021/acs.jmedchem.2c01599>.
51. de Chaumont, F., Dallongeville, S., Chenouard, N., Hervé, N., Pop, S., Provoost, T., Meas-Yedid, V., Pankajakshan, P., Lecomte, T., Le Montagner, Y., et al. (2012). Icy: an open bioimage informatics platform for extended reproducible research. *Nat. Methods* 9, 690–696. <https://doi.org/10.1038/nmeth.2075>.
52. Genin, P., Cuvelier, F., Lambin, S., Corte-Real Filipe, J., Autrusseau, E., Laurent, C., Laplantine, E., and Weil, R. (2015). Optineurin regulates the interferon response in a cell cycle-dependent manner. *PLoS Pathog.* 11, e1004877. <https://doi.org/10.1371/journal.ppat.1004877>.
53. Tan, V.P., Smith, J.M., Tu, M., Yu, J.D., Ding, E.Y., and Miyamoto, S. (2019). Dissociation of mitochondrial HK-II elicits mitophagy and confers cardioprotection against ischemia. *Cell Death Dis.* 10, 730. <https://doi.org/10.1038/s41419-019-1965-7>.

STAR★METHODS

KEY RESOURCES TABLE

| REAGENT or RESOURCE | SOURCE | IDENTIFIER |
|---|--|--|
| Antibodies | | |
| Anti-Optn | Generated in collaboration with the recombinant protein and antibodies platform (Farida Nato, Institut Pasteur) | D1.1 mAb, raised against GST-hOptn (aa 1–300) |
| Anti-Optn | Santa Cruz Biotechnology | Cat#sc-166576 (C2); RRID: AB_2156554 |
| Anti-pS342-Optn | Generated in collaboration with Eurogentec, purified with non phospho peptide- and phospho peptide-conjugated agarose gel. | Raised in rabbit using the sequence of a KLH- conjugated human phosphopeptide QALERKKnPSAIPSE. |
| Anti-PKC μ (PKD) | Santa Cruz Biotechnology | Cat#sc-935 (D-20); RRID: AB_2172390 |
| Anti-pS916-PKC μ (PKD) | Cell Signaling Technology | Cat#2051; RRID: AB_330841 |
| Anti-Phospho-(Ser/Thr) PKD Substrate (pMotif) | Cell Signaling Technology | Cat#4381; RRID:AB_1264239 |
| Anti-VSV tag | Abcam | Cat#ab50549 (P5D4); RRID: AB_883494 |
| Anti-SQSTM1/p62 | Santa Cruz Biotechnology | Cat#sc-28359 (D-3); RRID: AB_628279 |
| Anti-Tom20 | Santa Cruz Biotechnology | Cat#sc-17764 (F-10); RRID: AB_628381 |
| Anti-Parkin | Santa Cruz Biotechnology | Cat#sc-32282 (PRK8); RRID: AB_628104 |
| Anti-Parkin | Abcam | Cat#ab15494; RRID: AB_301903 |
| Anti-pS65-Parkin | Cell Signaling Technology | Cat#36866 |
| Anti-pS65-ubiquitin | EMD Millipore | Cat#ABS1513-I; RRID: AB_2858191 |
| Anti-Ubiquitin (pan) | Santa Cruz Biotechnology | Cat#sc-8017 (P4D1); RRID: AB_628423 |
| Anti-LC3 | MBL Int. Corporation | Cat#PM036; RRID: AB_2274121 |
| Anti-tubulin β | Sigma-Aldrich | Cat#T4026; RRID: AB_477577 |
| Anti-Flag | Merck | Cat#M2; RRID:AB_262044 |
| Anti-Mitofusin 2 (Mfn-2) | FabGennix | Cat#MIT2-201AP |
| Anti-PINK1 | Cell Signaling Technology | Cat#6946; RRID: AB_11179069 |
| Anti-VDAC1/Porin | Proteintech | Cat#55259-1-AP; RRID: AB_10837225 |
| Anti-TBK1 | Cell Signaling Technology | Cat#3013; RRID: AB_2199749 |
| Anti-NDP52/CALCOCO-2 | GeneTex | Cat# GTX115378; RRID: AB_10620266 |
| Anti-Mouse IgG (H + L) HRP | Jackson ImmunoResearch | Cat#31430; RRID: AB_10015289 |
| Anti-Rabbit IgG (H + L) HRP | Jackson ImmunoResearch | Cat#111-035-144; RRID: AB_2307391 |
| Anti-Goat IgG (H + L) HRP | Jackson ImmunoResearch | Cat#705-035-003; RRID: AB_2340390 |
| Anti-Mouse Alexa Fluor 488 | Life Technologies | Cat#A32723; RRID: AB_2633275 |
| Anti-Rabbit Alexa Fluor 488 | Life Technologies | Cat#A32731; RRID: AB_2633280 |
| Anti-Goat Alexa Fluor 488 | Life Technologies | Cat#A32814; RRID: AB_2762838 |
| Anti-Rabbit IgG Alexa Fluor 555 | Life Technologies | Cat#A21428; RRID: AB_141784 |
| Anti-Mouse Alexa Fluor 555 | Life Technologies | Cat#A21424; RRID: AB_141780 |
| Anti-Rabbit IgG2b Alexa Fluor 546 | Life Technologies | Cat#A21143; RRID: AB_1500891 |
| Anti-Rabbit IgG1 Alexa Fluor 488 | Life Technologies | Cat#A21121; RRID: AB_2535764 |
| Recombinant DNA | | |
| pMT-mKeima-Red | Obtained from Pr. Atsushi Miyawaki, RIKEN, Japan | |
| peBFP2-human PARK2 | Obtained from Pr. Wei Yuan Yang, Institute of Biochemical Sciences, Taiwan | |
| Parkin: pCMV- human PARK2 | Obtained from J Estaquier, Université de Paris, Paris, France | |

(Continued on next page)

Continued

| REAGENT or RESOURCE | SOURCE | IDENTIFIER |
|--|---|--|
| Catalytically dead version of Parkin: pCMV-human PARK2-C431S | Obtained from J Estaquier, Université de Paris, Paris, France | |
| pKillerRed-dMito | Erogen (Moscow) | Cat#FP964 |
| pVSV- human Optn wt and all Optn mutated forms | Generated in the laboratory | pcDNA3-VSV plasmid with G-VSV inserted at HindIII-XbaI of pcDNA3 |
| eGFP-PKD1 | Generated in the laboratory | peGFP plasmid with cDNA inserted at BglII-BamHI |
| GFP-Nterm fused to human PKD1 wild-type form | | |
| eGFP-PKD2 | Generated in the laboratory | peGFP plasmid with cDNA inserted at BglII-BamHI |
| GFP-Nterm fused to human PKD2 wild-type form | | |
| eGFP-PKD3 | Generated in the laboratory | peGFP plasmid with cDNA inserted at BglII-BamHI |
| GFP-Nterm fused to human PKD3 wild-type form | | |
| PKD1 pHA-human PKD1 wild-type form | Generated in the laboratory | pcDNA3-HA plasmid with T7-HA inserted at HindIII-XbaI of pcDNA3 |
| <i>Constitutively active version of PKD1:</i> PKD-CA pHA-human PKD1 constitutively active form - W538A substitution that releases the autoinhibitory domain. | Generated in the laboratory | pcDNA3-HA plasmid with T7-HA inserted at HindIII-XbaI of pcDNA3 |
| <i>Catalytically dead version of PKD1:</i> PKD-DN pHA-human PKD1 dominant negative form - K612W substitution located in the ATP binding pocket. | Generated in the laboratory | pcDNA3-HA plasmid with T7-HA inserted at HindIII-XbaI of pcDNA3 |
| pGST- human Optn and mutated/deleted versions | Generated in the laboratory | Backbone: pGEX-4T |
| pHA-Ub | Addgene | Cat#18712; RRID:Addgene_18712 HA-Ubiquitin insert from the human UBB gene in pcDNA3 |

Chemicals, peptides, and recombinant proteins

| | | |
|---|--------------------------|-----------------|
| FugeneHD | Promega | Cat#E2311 |
| Lipofectamine RNAiMAX | Invitrogen | Cat#13778150 |
| Alexa Fluor 488 Phalloidin | ThermoFischer Scientific | Cat#A12379 |
| Oligomycin A | Sigma-Aldrich | Cat#75351 |
| Antimycine A1 | Sigma-Aldrich | Cat#A8674 |
| 2-[2-(3-Chlorophenyl)hydrazinylidene] propanedinitrile (CCCP) | Abcam | Cat#ab141229 |
| Phorbol 12-myristate 13-acetate (PMA) | Sigma-Aldrich | Cat#P8139 |
| Ionomycin | Sigma-Aldrich | Cat#I9657 |
| Staurosporine | Sigma-Aldrich | Cat#S5921 |
| Hydrogen peroxide solution (H ₂ O ₂) | Sigma-Aldrich | Cat#H1009 |
| CID-2011756 (PKD inhibitor) | Sigma-Aldrich | Cat#SML0369 |
| CRT0066101(PKD inhibitor) | Sigma-Aldrich | Cat#SML1507 |
| BX795 (TBK1 inhibitor) | Sigma-Aldrich | Cat#SML0694 |
| Bafilomycin A1 | EMD Millipore | Cat#196000 |
| 3-Methyladenine (3-MA) | Sigma-Aldrich | Cat#M9281 |
| Tetramethylrhodamine, methyl ester (TMRM) | Invitrogen | Cat#I34361 |
| MitoSOX Dye | Invitrogen | Cat#M36009 |
| MitoTracker Green FM Dye | Invitrogen | Cat#M7514 |
| Fetal bovine serum | Gibco Life Technologies | Cat#11560636 |
| Penicillin/Streptomycin | Gibco Life Technologies | Cat#11548876 |
| Puromycin | Gibco Life Technologies | Cat#A1113803 |
| Geneticin (G418) | Gibco Life Technologies | Cat#10131035 |
| Proteases inhibitor/complete | Merck | Cat#11697498001 |
| Phosphatases inhibitor/PhosSTOP | Merck | Cat#4906845001 |

(Continued on next page)

Continued

| REAGENT or RESOURCE | SOURCE | IDENTIFIER |
|---|---|---|
| N-Ethylmaleimide (NEM) | Merck | Cat#128-53-0 |
| 2-Iodoacetamide (IAA) | Merck | Cat#I149 |
| 4-12% acrylamide precast gels | Biorad | Cat#3450124 |
| PVDF membranes | Millipore | Cat#Immobilon#IPVH00010 |
| Mowiol | Biovalley | Cat#17951-500 |
| DAPI | Sigma-Aldrich | Cat#D95-42 |
| Critical commercial assays | | |
| Bradford assay | Biorad | Cat#500006 |
| MycoAlert™ Mycoplasma Detection Kit | Lonza | Cat#LT07-318 |
| Duolink <i>In Situ</i> PLA | Sigma-Aldrich | Cat#DUO92004: Probe Anti-Mouse MINUS Cat#DUO92002: Probe Anti-Rabbit PLUS Cat#DUO92007: <i>In Situ</i> Detection Reagents Orange |
| Experimental models: Cell lines | | |
| HeLa cells | ATCC | Cat#CRM-CCL-2; RRID:CVCL_0030 |
| HeLa without exogenous expression | | |
| HEK293T cells | ATCC | Cat#CRL-3216; RRID:CVCL_0063 |
| U2OS cells | ATCC | Cat#HTB-96; RRID:CVCL_0042 |
| HeLa cells expressing Parkin | Engineered in the laboratory | |
| HeLa-mtKeima-Parkin cells that express untagged version of Parkin | | |
| HeLa cells expressing BFP-Parkin | Engineered in the laboratory | |
| HeLa cells that express eBFP-tagged Parkin | | |
| HeLa cells expressing mitochondria-targeted Keima and BFP-Parkin | Engineered in the laboratory | |
| HeLa cells that express a mitochondrial-targeted form of mKeima protein and eBFP-tagged Parkin | | |
| Parental HeLa TKO cells | Obtained from Pr. Richard Youle, National Institute of Neurological Disorders and Stroke, NIH, USA ⁵ | |
| HeLa Triple knockout (TKO) cells in which Optn, NDP52 and Tax1BP1 have been removed | | |
| HeLa TKO cells expressing mitochondria-targeted Keima and BFP-Parkin | Engineered in the laboratory | - |
| HeLa TKO-mtKeima-Parkin cells that express a mitochondrial-targeted form of mKeima protein and eBFP-tagged Parkin | | |
| SH-SY5Y cells | ATCC | Cat#CRL-2266; RRID:CVCL_0019 |
| SH-SY5Y cells expressing Mitokiller | Engineered in the laboratory | |
| SH-SY5Y cells that express a mitochondrial-targeted form of KillerRed protein | | |
| Oligonucleotides | | |
| TBK1 siRNA | Sigma Genosys | RNA duplexes synthesized with 2-nt (2'deoxy) uridine 3' overhang directed against nucleotides 1472 to 1492 for TBK1 (AAGCGGCAGAGUU AGGUGAAUAAA) |
| PKD1 siRNA | Dharmacon | Cat#M-005028-00 |
| PKD2 siRNA | Dharmacon | Cat#M-004197-01 |
| PKD3 siRNA | Dharmacon | Cat#M-005029-01 |
| Optn siRNA | Dharmacon | Cat#J-016269-05 Cat#J-016269-06 Cat#J-016269-08 |

(Continued on next page)

Continued

| REAGENT or RESOURCE | SOURCE | IDENTIFIER |
|--|---|---|
| Software and algorithms | | |
| FlowJo 10.0 software | BD Biosciences | https://www.appliedcytometry.com/ |
| AxioVisio software | Zeiss | https://www.micro-shop.zeiss.com/en/us/system/ |
| ImageJ/Fiji software | Fiji | https://imagej.net/software/fiji/downloads |
| CellProfiler software | Cimini Lab of the Broad Institute of MIT and Harvard. | https://cellprofiler.org/ |
| Other | | |
| T4 Cellometer cell counter | Nexcelom | |
| LB 941 Multimode Reader TriStar | Berthold Technologies | |
| Zeiss Axio Imager Z1 | Zeiss | https://www.originlab.com/origin |
| Olympus CK40 inverted | Olympus | |
| Chemidoc touch imaging device | Biorad | https://statistics.laerd.com/statistical-guides/one-way-anova-statistical-guide.php |
| LSRFortessa™ Cell Analyzer | Becton-Dickinson Biosciences | |
| Nikon Eclipse Ti2-E with spinning-disk CrestV3 | Nikon | |
| Software and algorithms | | |
| ICY program | Quantitative Image Analysis Unit, Institut Pasteur, bioimageanalysis.org ⁵¹ | |
| SODA ("Statistical Object Distance Analysis") | tool of the ICY software allows to map statistically coupled objects by calculating a pairing probability for each unique pair of objects | |
| JAMOVI software | The jamovi project, 2023, jamovi Version 2.3 | https://www.jamovi.org |
| Cell Profiler Software | Cell Image analysis software ²³ | https://cellprofiler.org |

EXPERIMENTAL MODEL AND STUDY PARTICIPANT DETAILS

The following commercial cell lines were used in this study: HeLa cells (ATCC, CRM-CCL-2), HEK293T cells (ATCC, CRL-3216), U2OS cells (ATCC, HTB-96), SH-SY5Y cells (ATCC, CRL-2266). HeLa Triple knockout (TKO) cells in which Optn, NDP52 and Tax1BP1 have been removed were obtained from Pr. Richard Youle (National Institute of Neurological Disorders and Stroke, NIH, USA). The following cell lines were engineered for this study: HeLa cells that express untagged or eBFP-tagged version of Parkin, HeLa cells that express a mitochondrial-targeted form of mKeima protein and eBFP-tagged Parkin, HeLa TKO-mtKeima-Parkin cells that express a mitochondrial-targeted form of mKeima protein and eBFP-tagged Parkin and SH-SY5Y cells that express a mitochondrial-targeted form of KillerRed protein.

Cell line authentication was performed through morphology checks utilizing a inverted microscope equipped with phase contrast capabilities. Cells were visualized under 10× and 20× magnification to assess morphological characteristics, including cell shape, size, and growth patterns. Any discrepancies or abnormalities observed were documented and compared against established reference images. Concurrently, mycoplasma contamination testing was conducted using Mycoplasma Detection Kit. Cell culture supernatants were collected and analyzed according to the manufacturer's instructions. Briefly, samples were mixed with substrate solution and incubated for 10 min at room temperature. Luminescence was then measured using a luminometer, with readings indicative of mycoplasma contamination levels. Authentication protocols were carried out routinely every two months to ensure the fidelity and purity of cell cultures used in experimental assays.

METHOD DETAILS**Cells and induction**

The different HeLa cell lines, Triple knockout (TKO) HeLa cells, HeLa WT or TKO-mtKeima-Parkin cells, U2OS and HEK-293T cells were grown in DMEM Glutamax (GIBCO) supplemented with 10% heat-inactivated FBS. Selection is maintained by addition of G418 (200 µg/mL) to the medium. SHSY5Y cells and SHSY5Y expressing mitochondrial KillerRed protein were maintained in RPMI1640 (GIBCO) supplemented with 10% FBS. Transient transfections of HeLa cell lines with siRNA and/or plasmids were performed using

Fugene HD or Lipofectamine RNAiMAX following the manufacturer's instructions. HeLa and HeLa-TKO cells stably expressing mitochondrial Keima and untagged or BFP-tagged Parkin were generated by transfection, selected with 200 µg/mL of Geneticin (G418) and 1 µg/mL puromycin and sorted by FACS.

For induction of mitophagy, cells were incubated in the presence of Oligomycin and Antimycin A1 (OA) at 10 µM each or CCCP (Carbonyl cyanide 3-chlorophenylhydrazone) at 20 µM for different times as indicated at 37°C. For inhibition of PDK and TBK1 kinase activities, cells were pre-treated either 45 min with 50 µM CID2011756 or 2h with 5 µM CRT0066101 or 1 µM of BX795 and induction was performed in the continuous presence of these drug. To confirm specificity of the mitophagy induction, HeLa cells were stimulated with OA in the presence of the autophagy inhibitors, 3-Methyladenine (3-MA, 5 mM) and baflomycin A1 (Baf, 200 nM). Activation of the PKD pathway was achieved using either oxidative stress (H_2O_2 , 10 µM, 15 min) or by well-known PKD activators such as Phorbol Myristate Acetate (PMA, 100 nM, 10 min) or Ionomycin (1 µM, 15 min).

Cell extracts, immunoprecipitations and immunoblots

Cells were lysed in a buffer containing 50 mM Tris, pH 7.5, 150 mM NaCl, 1% Triton X-100, 1 mM EDTA, phoSTOP, cOmplete and deubiquitinase inhibitors: 10 mM N-Ethylmaleimide (NEM) et 7 µM 2-Iodoacetamide (IAA). Protein concentrations in lysates were measured using Bradford assay. Clarified lysates or immunoprecipitates were mixed with 4X Laemmli buffer containing DTT and the samples were boiled for 10 min. Proteins were separated by SDS-PAGE using 4–12% acrylamide precast gels and transferred to PVDF membranes. Immunoreactive proteins were visualized by chemiluminescence. The chemiluminescence reaction was visualized and processed using ChemiDoc Imaging system. Immunoprecipitation assays were performed as previously described.⁵² For the relative quantification, densitometric analyses were performed using ImageJ Software. Band intensities in the linear range of the signal were measured using underexposed membranes. Two different concentrations of each sample were tested and samples with lower concentrations were used for densitometric analysis. For subcellular fractionations, mitochondrial and cytosolic extracts were obtained using a previously described protocol.⁵³

Kinase assay

Parental HEK293T cells or HEK293T cells transiently transfected with HA-PKD1 expressing plasmid were treated 10 min with Phorbol Myristate Acetate (PMA, 100 nM) and Ionomycin (1 µM) as indicated. When indicated Staurosporine (1 µM) was added for 1h prior to stimulation. For kinase assays, PKD was immunoprecipitated with anti-PKD antibodies and incubated with 1 µg GST-NEMO, GST-Optn, GST-Optn S342A, GST-Optn S415A or GST-Optn S342A/S415A proteins in kinase buffer 1X (50 mM Tris-HCl pH 7.5, 10 mM MgCl₂, 2 mM EGTA, phoSTOP from Roche) with 0.5 mM ATP and [γ -³²P] ATP for 30 min at 30°C. Immunoprecipitates were washed 3 times in kinase buffer and the reactions were stopped by the addition of 2X SDS sample buffer and analyzed by SDS-PAGE followed by autoradiography.

Immunofluorescence and *in situ* proximity ligation assay

For immunofluorescent experiments, fixation, permeabilization and image acquisition were performed as previously described.⁵² Staining of nuclei was performed with DAPI incubated for 5 min before mounting and cells were visualized by detection of actin protein using Alexa Fluor 488 Phalloidin. *In situ* PLA experiments, which enable the detection of protein interactions by producing a distinct, localized signal, were performed according to the instruction manual using mouse anti-Parkin and rabbit anti-VSV antibodies or rabbit anti-LC3 and mouse anti-Optn antibodies.

Measurement of mitophagy efficiency by the mitochondrial-targeted-Keima protein

Cells, cultured for 24 h, were transfected for 48 to 72 h and treated as described before cytometry. Analyses were performed on an LSR FORTessa cytometer. Measurements of lysosomal mitochondrial-targeted-mKeima were made using dual-excitation ratio-metric pH measurements at 440 nm (pH 7, violet laser) and 561 nm (pH 4, yellow-green laser) excitation (ex.) and 610/20 nm emission (em.) filters. For each sample, 100,000 events were collected and subsequently gated for BFP (ex. 405 nm, em. 450/50 nm)/mKeima double-positive cells. Data were analyzed using FlowJo (v10, Tree Star).

Measurement of the mitophagy process by flow cytometry

To measure mitochondrial membrane potential, 100 nM of Tetramethylrhodamine methyl ester (TMRM, Ex. 548 nm, Em. 574 nm) was preloaded into cells for 30 min. To measure the total mitochondrial global mass, cells were preloaded for 30 min with 200 nM MitoTracker Green FM (Ex. 490 nm, Em. 516 nm). For the measurement of mitochondrial ROS production, cells were treated with 500 nM MitoSOX (Ex. 396 nm, Em. 610 nm) for 30 min. Cells were washed twice in PBS prior to the emission measurement. Quantification of TMRM, MitoTracker and MitoSOX fluorescences were performed on an LSR FORTessa cytometer and data analyzed using FlowJo.

Live-cell imaging

HeLa cells expressing eBFP-Parkin and mitochondrial Keima were coated on µ-Slide 8 Well chambers 24h prior to imaging. Time-lapse imaging was performed using a confocal spinning-disk microscope. Images were acquired every 15 min for up to 4 h to monitor Parkin recruitment. Throughout the imaging session, focus drift was minimized using piezo autofocus systems, and phototoxicity was mitigated by optimizing laser power and exposure times.

QUANTIFICATION AND STATISTICAL ANALYSIS

Image processing and statistical analyses

Wildfield microscopy images were acquired using a fluorescent microscope. *In situ* PLA hybridization signals and measurement of Parkin recruitment to damaged mitochondria were obtained using a confocal spinning-disk microscope (objective x100 NA 1.45). For each condition, five images with 5–10 z-stacks were acquired.

Statistical analyses of Parkin and Optn localization were performed using ICY program. The SODA (“Statistical Object Distance Analysis”) tool of the ICY software allows to map statistically coupled objects inside the cell, by calculating a pairing probability for each unique pair of objects.²¹ The average statistical distances between Optn and Parkin have been calculated and the coupling percentage is represented as a function of the distance (in pixels) between two points. This method is suitable for analyzing microscopy images of wild-field samples.

The assessment of Parkin recruitment to damaged mitochondria during mitophagy relied on quantifying the colocalization of Parkin and mitochondria signals. Pearson and Manders coefficients were calculated using the ICY software, specifically employing the co-localization studio module. These coefficients provided quantitative measures of the degree of overlap between Parkin and mitochondria fluorescence signals.

The Jamovi Software (The jamovi project, 2023, jamovi Version 2.3, <https://www.jamovi.org>) was used to determine statistical significance. Descriptive statistics and graphs indicated parametric ANOVA tests. The Fisher tests were significant. A 2-to-2 comparisons were performed to identify significant differences, using Tukey's post-hoc test. "n.s." denotes not statistically significant, * $p < 0.05$, ** $p < 0.01$, *** $p < 0.001$.

Line scans

In Fiji Software, line scans were generated using a three-pixel line width to trace TOM20-labelled mitochondria. Intensity values were normalized by dividing the dataset by its average, except for TOM20 signal that was normalized by dividing by its maximum to facilitate the visualization of Parkin and Optn signals.

Immunoblotting quantification

Immunoblot bands were quantified using Fiji Software. For each condition, band intensities of phosphorylated form and total protein corresponding to the same lane were quantified and the ratio between the two values was represented. Experiments were performed at least in duplicate.